이학박사학위논문

I. Studies on the efficient organic reactions based upon palladium nanocrystals

II. Design and synthesis of novel blue phosphorescent host materials for organic light-emitting diode application

I. 팔라듐 나노결정를 이용한 효과적인 유기 반응 개발

II. 유기 발광 다이오드에 응용 가능한 신규 청색 인광 호스트 물질의 설계 및 합성

2014년 2월

서울대학교대학원
화학부유기화학전공
정주영

CONTENTS

II. Design and synthesis of novel blue phosphorescent host materials for organic light-emitting diode application

Abstract

I. Studies on the efficient organic reactions based upon palladium nanocrystals

In organic synthesis, palladium has been used as one of the key transition metal catalysts for various functional group transformations and C-C bond forming reactions. Despite the importance of palladium-catalyzed reactions, reactions employing the homogeneous palladium catalysts are often associated with significant problems including instability of the catalyst in air, toxicity caused by residual metal species, safety issues, high cost and scarcity of the metal. These shortcomings have impeded their general application in industry. To overcome these drawbacks, researchers have developed heterogeneous palladium catalysts. However, reactions using heterogeneous catalysts are often accompanied with reduced activity and selectivity compared with those of homogeneous catalysts. As a result, heterogeneous catalyst systems have a restrictive substrate scope or need harsher reaction conditions. Therefore it would be ideal to devise new types of catalysts that can maximize the benefits of both homogeneous and heterogeneous catalysts and minimize the shortcomings of either. As a way of achieving this goal, many researchers suggested the nanocrystals for catalysts. Nanocrystals have high surface area per volume and good dispersive property that can lead to high catalytic activity like homogeneous catalysts. Furthermore they could be handled like heterogeneous catalysts. Due to these characteristics, nanocrystal catalysts are called semi-heterogeneous catalysts and have desirable attributes of both systems, i.e. the efficiency of homogeneous reactions and the recyclability of the heterogeneous materials.

In chapter I, we report the results of our investigation on the use of filtration free, magnetically separable Pd-Fe_3O_4 nanocrystal catalysts for

several cross coupling reactions. After each reaction, the nanocrystals can be separated from the reaction mixture most conveniently through the use of an external magnet. Recovered catalysts show highly conserved reactivity and the reactions employing the nanocrystals exhibit a wide substrate scope. The efficiency, operational simplicity, cost effectiveness, and environmentally benign features of the present Pd-Fe_3O_4 catalyst system lend itself an opportunity to be extended to large-scale applications including industrial processes. Our current efforts are aimed at exploring the full potential and the detailed mechanistic aspects of the reactions employing the nanoparticle catalysts.

The catalytic properties of metal nanocrystals can be drastically altered through the control of their shapes, which determine surface atomic arrangements and thus affect activity and/or selectivity toward a specific catalytic reaction. In chapter II, we demonstrate that in the alkyne hydrogenation, extremely high *cis*-alkene selectivity can be achieved simply by shaping Pd nanocrystals to expose metal facets that favor the adsorption of alkynes compared to alkenes. In this work, we synthesized Pd nanocrystals with a cubic shape and thus possessing exposed {100} facets and then applied them to selective semihydrogenation of various alkynes. Our approach based on the shape control of Pd nanocrystals offers a simple and effective route to develop a highly selective catalyst for alkyne semihydrogenation.

Key words: Heterodimeric nanocrystals; Palladium nanoparticle; Pd-Fe_3O_4, Cross-coupling reaction; Suzuki coupling; Heck reaction; Sonogashira reaction; C-H activation; Catalyst; Magnetic separation; Recycling; Shape-controlled nanocrystals; Nanocube; Alkyne hydrogenation

II. Design and synthesis of novel blue phosphorescent host materials for organic light-emitting diode application

Organic light-emitting diode (OLED) is considered next generation technology for lighting and panel displays because of their full-color emission, low driving voltages, rapid responses, low power consumptions and high contrasts. OLED also has self-luminescent capability, not needing extra backlight. Devices based on the OLED's can be as thin as 1 mm, much thinner than that of the Liquid Crystal Display (LCD), which has been the major display technology so far. Furthermore, OLED's have simple manufacturing process and could be implemented as portable and/or flexible display.

However, even with all the advantageous features of the OLED, blue phosphorescence is still under development and further progress on the materials development for high triplet energy charge transport is in dire need. For commercialization, new design and synthesis of stable and efficient blue phosphorescence materials are needed. The presently available materials do not have enough thermal and morphological stability and quantum efficiency. Therefore, novel host materials are needed to satisfy the required specifications. In this study, we designed novel compounds for blue phosphorescent host materials, which exhibit high triplet energy level, high electron/hole transportation property and high mobility. The main goal is development of new types of bipolar host materials, which have both electron donor and acceptor in a single molecule.

Totally 29 new compounds were synthesized and 24 compounds were evaluated as host materials. Some of these compounds showed superior luminous and power efficiencies, as well as the deep blue color in CIE coordinates, compared to existing OLED materials.

Key words: OLED, phosphorescence, host materials, bipolar structure, carbazole; device performance

List of Figures

Figure I-10. Br 3d XPS core level spectrum taken from the Pd nanocubes after extensive washing with ethanol and water. In the spectrum, the Br $3d_{5/2}$ and Br $3d_{3/2}$ binding energies were 67.6 and 68.5 eV, respectively, which were close to the literature values for Br^-.

Figure I-11. Hydrogenation of 5-decyne on 2.0 mol% Pd/C catalyst that were pre-treated with bromide ions. The pre-treatment was conducted by heating 11 mL of an aqueous mixture containing the commercial Pd/C catalyst (200 mg) and KBr (200 mg) at 80 ^oC for 3 h.

Figure I-12. Illustrations of the lowest energy adsorption modes of acetylene and ethylene on Pd(100) and Pd(111): a) acetylene on a 4-fold hollow site of Pd(100); b) ethylene on a 2-fold aligned bridge site of Pd(100); c) acetylene on a 3-fold hcp site of Pd(111); and d) ethylene on a 2-fold aligned bridge site of Pd(111).

Figure II-1. Common blue phosphorescent dopant materials: (a) Firpic and (b) Fir6

Figure II-2. Commonly used host materials for OLED.

Figure II-3. The concept of bipolar host materials

Figure II-4. Synthesized compounds containing oxadiazole unit.

Figure II-5. Synthesized compounds containing triazole unit.

Figure II-6. UV–vis absorption, PL spectra of compound **34**

List of Schemes

List of Tables

Part I.

I. Studies on the efficient organic reactions based upon palladium nanocrystals

Chapter 1. Catalytic applications of Pd–Fe_3O_4 heterodimeric nanocrystal to magnetically recyable catalysts for cross-coupling reactions

1. Introduction

In organic synthesis, palladium is one of the key metal catalysts for various functional group transformations and C-C bond forming reactions. In this regard, it is of particular note that the chemists who contributed to the development of the cross coupling reactions using palladium catalyst such as Heck, Suzuki and Negishi reactions won the Nobel prize in 2010.[1] Many other related cross coupling reactions have been developed along with the three representative named reactions. In addition, many palladium-catalyzed reactions were reported for other, non-coupling reactions such as reduction and oxidation.[2] The organic reactions using palladium as catalysts are well documented in many reviews and books.[3]

Despite the importance and wide usage of palladium-catalyzed reactions, the homogeneous palladium catalysts have significant problems including instability in air, toxicity caused by residual metal species, safety issue and high cost due to scarcity of the metal, which have impeded their general application in industry.[4] To overcome these drawbacks, several researchers have developed heterogeneous palladium catalysts.[5] The heterogenization methods have usually employed biphasic systems or immobilization on supports. There are examples of biphasic systems that use separable ionic liquids[6] or phase transfer methods.[7] In case of immobilization, materials such as carbon nanotubes, graphene, high-surface area solids (silicates, alumina, zeolites, etc.), polymers, and metal oxides have been reported for supporters.[8] Heterogeneous catalysts have several advantages: 1) easy recovery and handling, 2) recyclable catalytic materials, 3) low metal residue in products. Such advantages render the heterogeneous catalysts suitable for the bulk synthesis and industrial applications. Especially, reduced metal contents of the products are particularly important issue in pharmaceutical industry.

However, the reactions using heterogeneous catalysts are often associated with reduced activity and selectivity compared with those using homogeneous catalysts. As a result, heterogeneous catalyst system may have restrictive substrate scope or need harsher conditions. Therefore it would be ideal to devise new types of catalysts that can maximize the benefits of both homogeneous and heterogeneous catalysts and minimize the shortcomings of either. As a way of achieving this goal, many researchers suggested the nanocrystals for catalysts.[9] Nanocrystals have high surface area per volume ratio and good dispersive property that can lead to high catalytic activity like homogeneous catalysts. Furthermore they could be handled like heterogeneous catalysts. Due to these characteristics, nanocrystal catalysts are called semi-heterogeneous catalysts and have desirable attributes of both systems, i.e. the efficiency of homogeneous reactions and the recyclability of the heterogeneous materials. Therefore interest in nanocrystals catalysis has been increasing gradually, and a large number of related research results have been reported in the last decade.[10]

Recently, synthesis and application of hybrid nanocrystals composed of two or more different materials have been reported beyond simple metal nanocrystals.[11] Properties of individual metal nanocrystals can be exploited in hybrid nanocrystals, possibly leading to synergistic and enhanced characteristics. Among them, heterodimeric nanocrystals composed of transition metals and oxides have been synthesized and used to multifunctional applications including biomedical sensing and catalytic reactions.[12]

However, in many cases, syntheses of heterodimer nanocrystals need several complex steps. Furthermore isolation and recovery process of these tiny nanocrystals from the reaction mixture is often not straightforward. To overcome these problems, we report the simple synthesis of Pd-Fe_3O_4

heterodimer nanocrystals through controlled, one-pot thermal decomposition of metal acetylacetonato mixture solution. The heterodimer nanocrystals are composed of a 6 nm-sized Pd nanosphere and a 30 nm-sized faceted Fe_3O_4 nanocrystal and they are soft ferrimagnetic with high saturation magnetization and low coercivity values. A sufficient amount of nanocrystals could be obtained in a gram-scale by simple synthetic method. They can be easily recovered using an external magnet without filtration or centrifugation process.

Herein, we describe the catalytic applications of Pd-Fe_3O_4 heterodimeric nanocrystals.[13-16] Pd-Fe_3O_4 heterodimeric nanocrystals have exhibited consistently high catalytic activities in many organic reactions, particularly in the absence of extra ligands. This efficient and cleanly reusable nanocrystal catalyst system is expected to reduce additives and increase the atom efficiency for greener chemistry. Also it is acceptable for industrial application, because of its potential to be scaled up.

2. Results and Discussion

We performed a series of representative coupling coupling reactions to test the catalytic activity of the Pd–Fe_3O_4 heterodimer nanocrystals.[13] It was found that the Pd–Fe_3O_4 heterodimer nanocrystals have excellent catalytic activity for Suzuki coupling reactions of phenylboronic acid with various aryl iodides, although less activated aryl bromide showed lower activity (Table 1). The nanocrystal catalyst also showed excellent catalytic activity for Suzuki coupling reactions of various substituted arylboronic acids with iodobenzene.

Table 1. Summary of Suzuki coupling reaction of arylboronic acid with aryl halide.

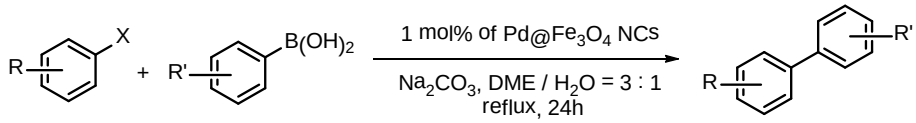

Entry	Aryl boronic acid	Aryl halide	Yield(%)[a]
1	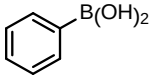		99(92[a])
2	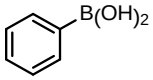	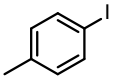	98
3	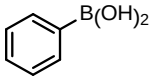	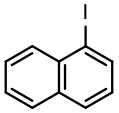	98
4	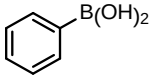	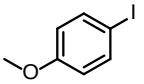	95
5	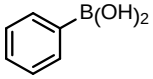	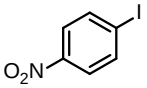	92
6	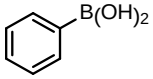	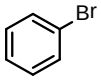	70
7	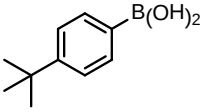	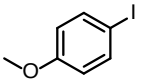	99
8	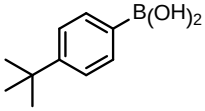		97
9	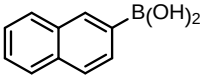		96
10	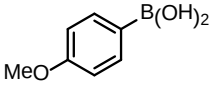		93
11	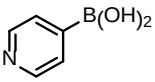		91
12	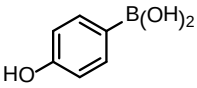		83

* All the reactions were carried out with 1.0 mmol of aryl halide, 1.2 equiv of arylboronic acid, and 1.3 equiv of sodium carbonate in 3 mL of DME and 1 mL of deionized water.
* All the yields are isolated yields of purified products.
[a] This reaction was performed using 0.1 mol% of the catalyst during 48 h reaction.

To overcome the intrinsic difficulty associated with the separation of both homogeneous palladium complex based catalysts and Pd nanoparticle-based catalysts from various carbon–carbon coupling reactions, we have immobilized palladium nanoparticles on magnetic materials to impart magnetic separation capability for easy recovery and recycling of the catalysts. When the Suzuki reaction of phenylboronic acid with iodobenzene was completed, the Pd–Fe_3O_4 heterodimer nanocrystals could be easily separated from the reaction mixture using a magnet, and the nanocrystal catalyst could be recycled many times without losing the catalytic activity. As shown in Table 2, the catalyst showed excellent catalytic activity even after 10 times of recycling.

Table 2. Recycling results on the coupling reaction of phenylboronic acid with iodobenzene

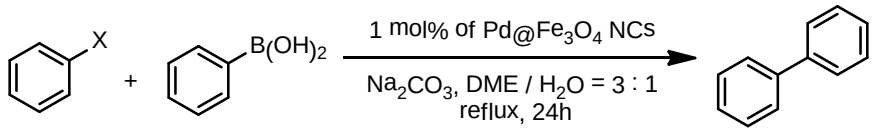

Run	1st	2nd	3rd	4th	5th	6th	7th	8th	9th	10th
Yield(%)	93	92	94	90	92	96	92	92	90	91

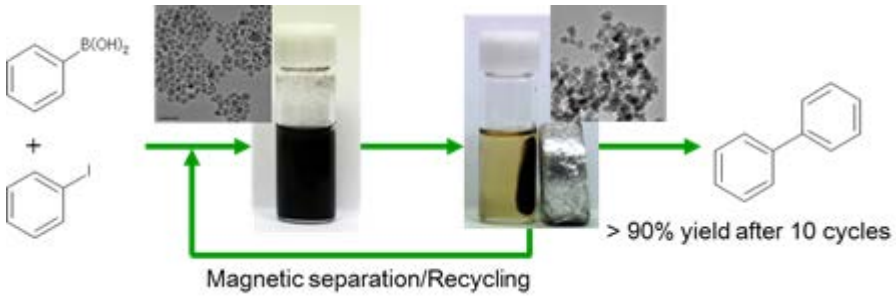

Figure 1. Magnetic separation and recycling of the Pd-Fe_3O_4 heterodimer nanocrystal catalyst

We investigated the catalytic performance of the Pd–Fe_3O_4 heterodimer nanocrystals for Suzuki coupling reactions of aryl bromides with phenylboronic acids. Under the identical reaction conditions as those used for aryl iodides, only 70% yield was obtained (Table 1, entry 6). To optimize the reaction conditions, various combinations of solvents and bases have been tried and the best result was obtained when 1,4-dioxane was employed as a solvent with K_3PO_4 as a base (Table 3). When the Suzuki coupling reactions of various substituted aryl bromides with phenylboronic acid were performed, good catalytic activities were observed (Table 4).

Table 3. Optimization of Suzuki coupling reaction

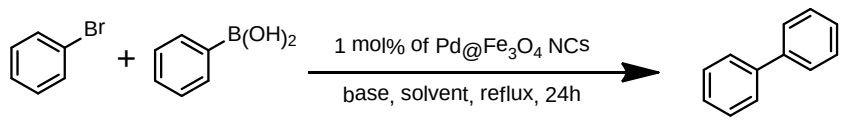

Entry	Aryl bromide	Product	Yield(%)
1	DME/H2O(3:1)	Na_2CO_3	70
2	isobutanol	Na_2CO_3	trace
3	2-methoxyethanol	Na_2CO_3	32
4	DMF	Na_2CO_3	35
5	1,4-dioxane	Na_2CO_3	65
6	2-methoxyethanol	K_3PO_4	26

7	1,4-dioxane	K_3PO_4	80

* All the reactions were carried out with 1.0 mmol of bromobenzene, 1.2 equiv of phenylboronic acid, and 1.3 equiv of base in 3 mL of solvent.
* All the yields are isolated yields of purified products.

Table 4. Summary of the Suzuki coupling reaction of phenylboronic acid with various aryl bromide

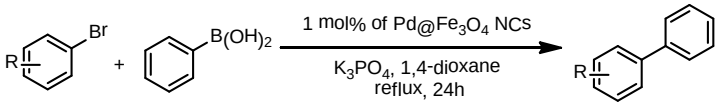

Entry	Aryl bromide	Product	Yield(%)
1	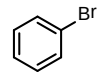	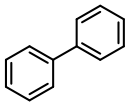	81
2	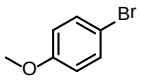	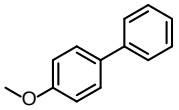	72
3	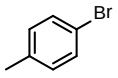	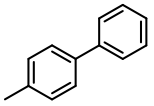	71
4	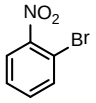	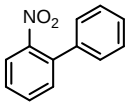	77
5	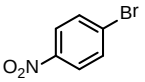	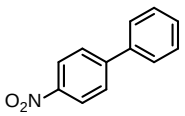	87

Various reaction conditions were tested for the investigation of the catalytic activity of the Pd–Fe_3O_4 heterodimer nanocrystals toward Heck and Sonogashira reactions and a particular attention was given to address if additives were necessary for the reactions.[14] It was found that without any additives the nanocrystal catalyst showed good catalytic activity for Heck and Sonogashira reactions (Scheme 1). In the original Sonogashira reaction,

coupling of terminal alkynes and aryl halides was reported to be catalyzed by a palladium(0) reagent in the presence of copper(I) co-catalyst. In many homogeneous palladium-catalyzed reactions it has been necessary to employ several additives such as phosphine or amine ligands for proper reactivity. In relation to this, a number of ligand-free Heck reactions and copper-free Sonogashira reactions have been investigated. However, still the use of several types of additives such as surfactants or metal salts has been reported to be necessary. In these cases, though additives help to promote the catalytic activity, they produce unwanted waste and sometimes byproducts. Our heterodimeric nanocrystal Pd–Fe_3O_4 catalyst system was found to be very effective in reducing reaction waste since it does not require any additives other than the base.

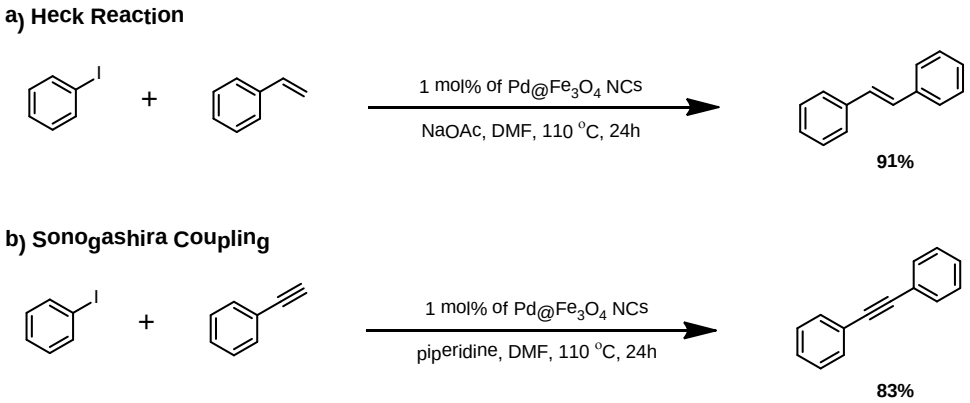

Scheme 1. C-C cross coupling reactions using Pd-Fe_3O_4 nanocrystals

To establish the scope of the catalytic system for Heck reactions we have screened various substrates using styrene or *tert*-butyl acrylate as an olefin counterpart (Table 5). The results showed acceptable yields of the Heck products from the reactions with aryl iodides having electron-rich or electron-poor substituents (entries), except for the case of 1-iodonaphthalene, where 46% yield was obtained (Table 5, entry 3). Most reactions using styrene or *tert*-

butyl acrylate and aryl iodides gave good yields regardless of the position of the substituent. However, reactions with aryl bromides gave slightly lower yields leaving some unreacted starting materials. Therefore we have screened further reaction conditions and better results were observed in DMA at 150 ^{o}C

Table 5. Investigation of ligand-free Heck reactions

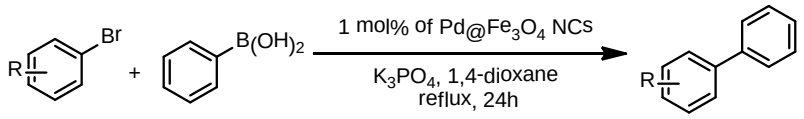

Entry	Substrate	Aryl bromide	Product	Yield(%)[a]
1			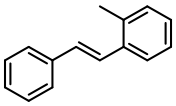	81
2		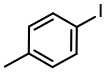	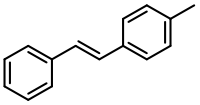	78
3		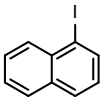	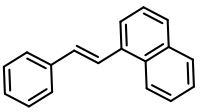	46(70)
4		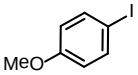	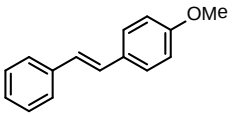	79
5	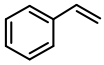	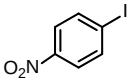	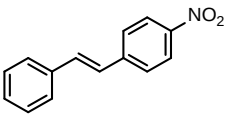	83
6		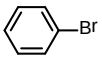	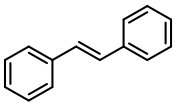	76(89)
7		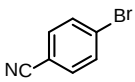	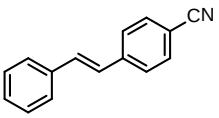	78(88)

8		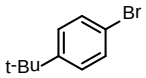	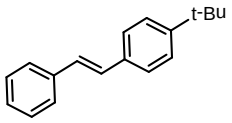	71(85)
9	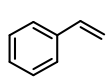	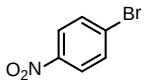	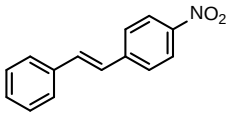	74(89)
10			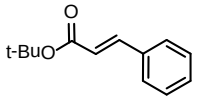	88
11	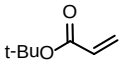		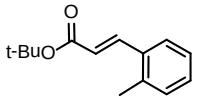	85
12		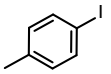	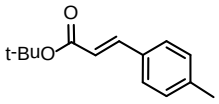	82
13		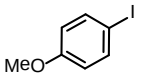	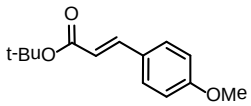	82

[a] Numbers are yields of purified products. Values in parentheses are yields of reactions performed in N,N-diemthylacetamide (DMA) at 150^{o}C.

When the same Pd–Fe_3O_4 heterodimeric nanocrystals were employed as catalysts for Sonogashira reactions using phenylacetylene or 4-methoxyphenylacetylene as representative alkynes, the reactions proceeded smoothly (Table 6).

Table 6. Substrate scope for Sonogashira reactions

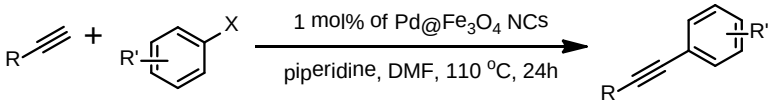

Entry	Substrate	Aryl bromide	Product	Yield(%)[a]

1	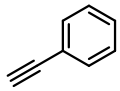		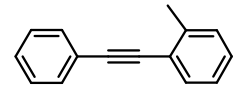	78
2		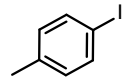	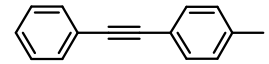	74
3		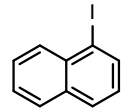	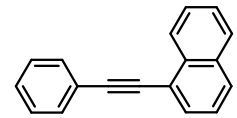	58(70)
4		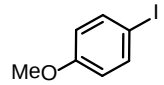	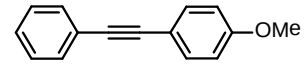	78
5	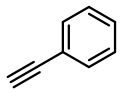	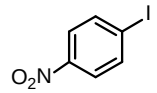	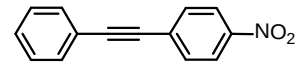	74
6		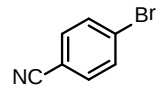	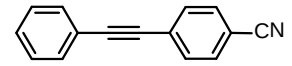	52(71)
7		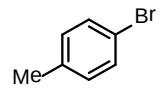	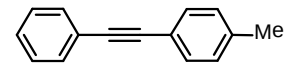	62(76)
8		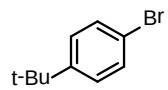	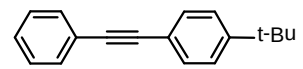	66(78)
9		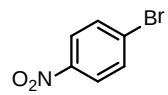	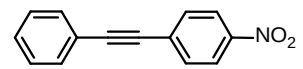	59(70)

10			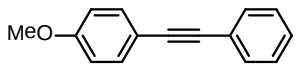	81
11	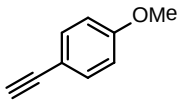		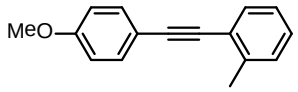	78
12		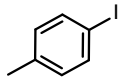	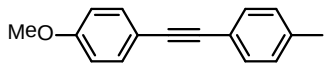	73
13		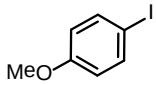	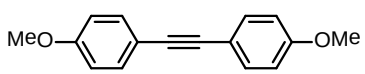	83

[a] Numbers are yields of purified products. Values in parentheses are yields of reactions performed in N,N-diemthylacetamide (DMA) at 150^{o}C

Again, most of the reactions exhibited acceptable levels of yields with aryl iodides except for the reaction with 1-iodonaphthalene (58% yield, Table 5, entry 3). Similar to the cases of Heck reactions, better results were observed in DMA at higher reaction temperatures for aryl bromides.

Reuse of the recovered catalyst particles was investigated in both Heck and Sonogashira reactions in Scheme 1. As shown in Table 6, the nanocrystals can be reused six times without loss of its catalytic activity for both Heck and Sonogashira reactions. To test the potential for practical synthetic applications, we carried out a larger scale Heck reaction as shown in Scheme 1 and the 10 mmol scale reaction proceeded smoothly, giving 90% yield of the desired product.

Table 7. Recycling results on Heck and Sonogashira reactions[a]

Entry	Reactions	Number of runs	Yield (%)[b]
1	Heck reaction	1	91

		2	90
		3	90
		4	91
		5	92
		6	89
2	Sonogashira reaction	1	83
		2	82
		3	83
		4	85
		5	82
		6	81

[a] Both reactions were performed under the same conditions as in Scheme 1.
[b] Numbers are the yields of isolated and purified products.

Our exploration began with screening various parameters of the cross-coupling reaction between imidazo[1,2-a]pyridine and 4-bromonitrobenzene employing phosphine-free conditions (Table 8).[15] When a 1.5:1mixture of imidazo[1,2-a]pyridine and 4-bromonitrobenzene in DMA was heated under reflux (166 ^{o}C) in the presence of Pd-Fe_3O_4 nanocrystals (1 mol % in Pd) and NaOAc (2 equiv), the reaction was completed in 12 h to give rise to the C3-arylated product exclusively in 88% yield (Table 8, entry 1). Similarly, the reactions employing KOAc or CsOAc as a base also gave C3-arylated product, albeit in lower yields (Table 8, entries 2and 3). In contrast, the use of AgOAc resulted in a very low conversion, and C3-arylated product was obtained only in a yield of 5% from a sluggish reaction (Table 8, entry 4). Various carbonate bases were also examined, and K_2CO_3 proved to be the most effective (Table 8, entries 5-7). It was notable that Na_2CO_3 performed poorly vis-a-vis NaOAc, whereas K_2CO_3 and KOAc gave comparable results (Table 8, entries1 and 2 vs 5 and 6). In a brief survey of solvents, *N*-methyl-2-pyrrolidone (NMP) was found to be equally effective as DMA while the reaction in *N*,*N*-dimethylformamide (DMF) led to a significant decrease in both the reaction

rate and yield. It should be noted that in contrast to the report on arene C-H arylation,[17] the Pd-Fe_3O_4 nanocrystals were absolutely necessary for this heteroarene C-H arylation reaction as verified by a control experiment where no reaction occurred in the absence of Pd-Fe_3O_4 or in the presence of only Fe_3O_4 even at a higher reaction temperature for a prolonged reaction time. The arylation was also performed with chloro- and iodo- substrates for comparison with bromide. Though 4-chloronitrobenzene did not undergo the arylation but instead decomposed slowly under the conditions of entry 1, the reaction of 4-iodonitrobenzene was completed in 9 h to produce the desired product in 87% yield, indicating the differential reactivity of aryl halides in this process.

Table 8. Direct arylation of imidazo[1,2-a]pyridine with 4-bromo nitrobenzene

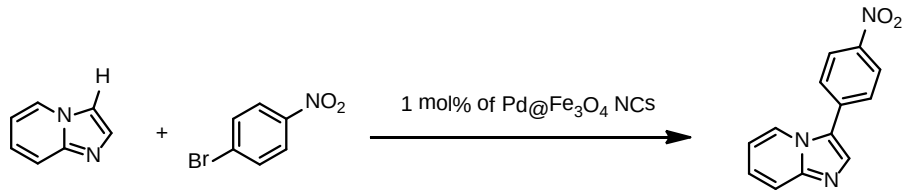

Entry	Solvent	Base	Temp.(°C)	Time(h)	Yield(%)
1	DMA	NaOAc	166	12	88
2	DMA	KOAc	166	12	75
3	DMA	CsOAc	166	12	62
4	DMA	AgOAc	166	18	5
5	DMA	Na_2CO_3	166	30	30
6	DMA	K_2CO_3	166	12	82
7	DMA	Cs_2CO_3	166	12	58
8	DMF	NaOAc	120	21	12
9	NMP	NaOAc	166	12	87

10	NMP	NaOAc	180	10	88

* All reactions were carried out with 4-bromonitrobenzene (0.50 mmol), imidazo[1,2-a]pyridine (0.75 mmol), base (1.0 mmol), and Pd–Fe3O4 (0.005 mmol, 1 mol % in Pd) at 0.25 M concentrations.

Having established the viability of Pd-Fe_3O_4 nanocrystals as the catalyst to effect the direct C-H arylation of imidazo[1,2-a]pyridine, we set out to examine the scope of the reaction. It was found that the conditions were general and efficient with a wide range of aryl bromides (Table 9). Under the optimal conditions derived from screening experiments (1.0 mol % Pd catalyst, NaOAc, DMA, 166 ^{o}C,12 h), aryl bromides having differential electronic and steric properties participated well in the cross-coupling reaction with imidazo[1,2-a]pyridine to afford the corresponding C3-arylated products. In no case, was detected the formation of other regioisomers including the C2-arylated product. While electron-poor (Table 9, entries 1-4) as well as electron-rich (Table 9, entry 6) aryl bromides underwent the direct C-H arylation, the reaction of the latter was less efficient, giving a low yield. A variety of functional groups, such as nitrile, aldehyde, ketone, chloride, and ether were tolerated. When the reaction was performed with 4-bromochlorobenzene, the desired arylated product (Table 9, entry 4) was produced in 67% yield with the chloride group unaffected, suggesting the possibility of carrying out an additional cross-coupling process. The C-H arylation reaction was insensitive to the substituent present in aryl bromides as shown by the comparable outcomes from the reactions of para- and meta-substituted aryl bromides (Table 9, entries 1 and 2 vs. 7 and 8). Furthermore, polycyclic aryl bromides including ortho-fused substrates could also be successfully employed for the reaction (Table 9, entries 9-11). In these reactions, both 1- and 2-bromonaphthalenes proved to be equally competent participants of the cross-coupling reaction with imidazo[1,2-a]pyridine to furnish arylated product (Table 9, entries 9-10), respectively. It was worthy of note that 9-bromoanthracene, a substrate with high steric congestion, was also

found to be suitable for the reaction, furnishing the anthracenylated product in 58% yield (Table 9, entry 11).

Table 9. Scope of the direct arylation of imidazo[1,2-a]pyridine with aryl bromides

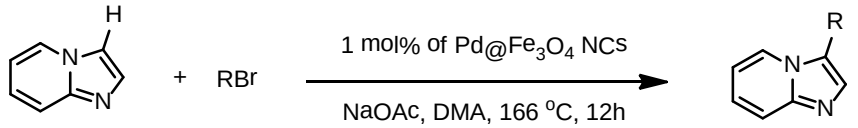

Entry	Aryl bromide	Yield (%)
1	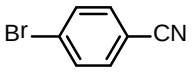	95
2	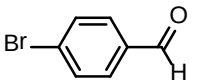	82
3	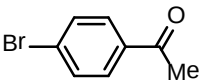	94
4	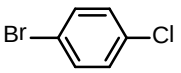	67
5	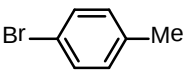	81
6c	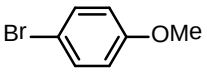	42
7	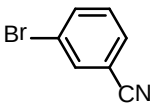	94
8	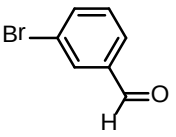	74

9	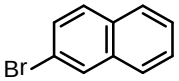	75
10	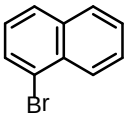	70
11	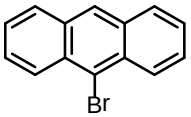	58

* All reactions were carried out with imidazo[1,2-a]pyridine (0.75 mmol), aryl bromide (0.50 mmol), NaOAc (1.0 mmol), and Pd–Fe_3O_4 (0.005 mmol, 1 mol % in Pd) in DMA (0.25 M) at 166 °C for 12 h.

We investigated other heteroarene C-H arylation reaction with aryl bromides. Under the identical reaction conditions as those used for imidazo[1,2-a]pyridine, some heteroarenes gave the arylated products without other regioisomers (Scheme 2).

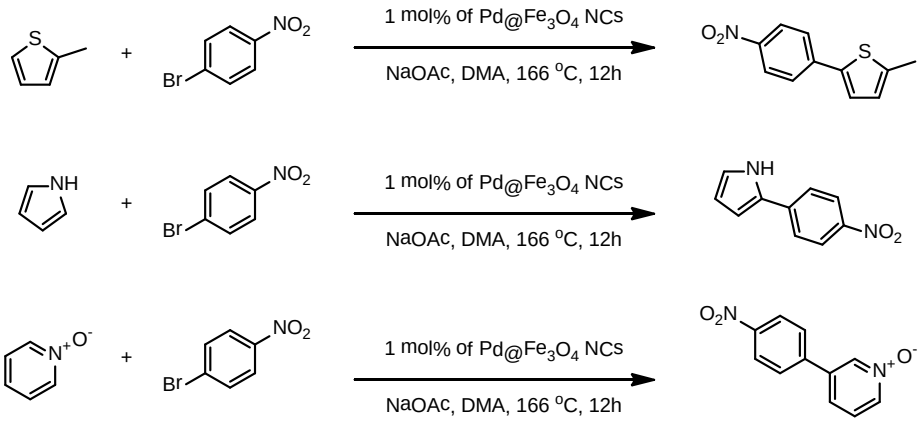

Scheme 2. Direct arylation of heteroarenes

As other reactions using the Pd-Fe_3O_4 nanocrystals, the recovery and recycle of nanocrystals were performed in direct arylation of heteroarene. We carried out a set of catalyst recycling experiments as shown in Table 10. Under the standard conditions, the cross-coupling reaction of imidazo[1,2-

a]pyridine with 4-bromonitrobenzene was repeated using the nanocrystals that were recovered each time from the previous run. Remarkably, the catalytic activity was found to remain unaltered throughout 10 runs to produce the same level of high efficiency (average yield 85%). In these recycling experiments, more than 98% of the nanocrystals could be recovered through a simple procedure involving separation by an external magnet and catalyst purification by dispersion-collection cycles.

Table 10. Recycling of the Pd–Fe_3O_4 nanocrystals for the direct arylation of imidazo[1,2-a]pyridine

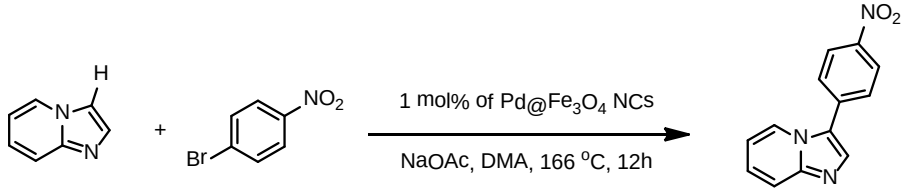

Run	1	2	3	4	5	6	7	8	9	10
Yield(%)	88	87	83	85	85	84	85	84	87	86

To explore the leaching of Pd from the nanocrystal catalyst, the concentration of Pd in the Pd–Fe_3O_4 heterodimer nanocrystals was obtained by using inductively coupled plasma atomic emission spectroscopy (ICP-AES) analysis. The relative Pd concentrations in the catalyst before the reaction and after 10 cycles of the Suzuki coupling reactions were almost not changed. The ICP-AES data of palladium in the product solution after one reaction followed by subsequent magnetic separation revealed that Pd concentration was within the detection limit. These data demonstrate that hardly any Pd leached out.

After one cycle of the catalytic reaction, we performed thermogravimetric analysis (TGA) and Fourier transform infrared (FT-IR) spectroscopy analysis. The FT-IR spectra show that the transmittance peaks of the N–H bond of the oleylamine surfactant decreased after the catalytic reaction (Fig. 2a). In

addition, the TGA data show that there is a slight weight loss of the catalysts after the catalytic reaction, due to the removal of oleylamine (Fig. 2b). These results show that although the Pd catalysts were stable and hardly leached out after several cycles of catalytic reaction, the surfactants around Pd nanocrystals were partially removed during the catalytic reaction.

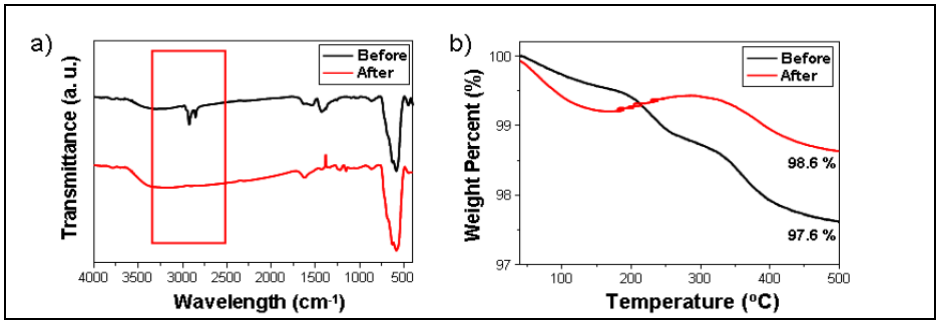

Figure 2. a) FT-IR spectra and b) TGA curves of Pd-Fe3O4 heterodimer nanocrystals after one cycle of catalytic reaction

Figure 3 shows properties of the catalysts before and after recycling runs of catalytic reaction. In transmission electron microscope (TEM) images, Pd nanosphere and faceted Fe_3O_4 heterodimeric nanostructure in both samples appear almost unchanged in their size and shape (Fig. 3a and 3b). Also magnetic behavior (Fig. 3c and 3d) and X-ray diffraction (XRD) patterns (Fig. 3e and 3f) of both samples confirmed their physicochemical stability. These results explain the uniform catalytic activity even after 10 times of recycling.

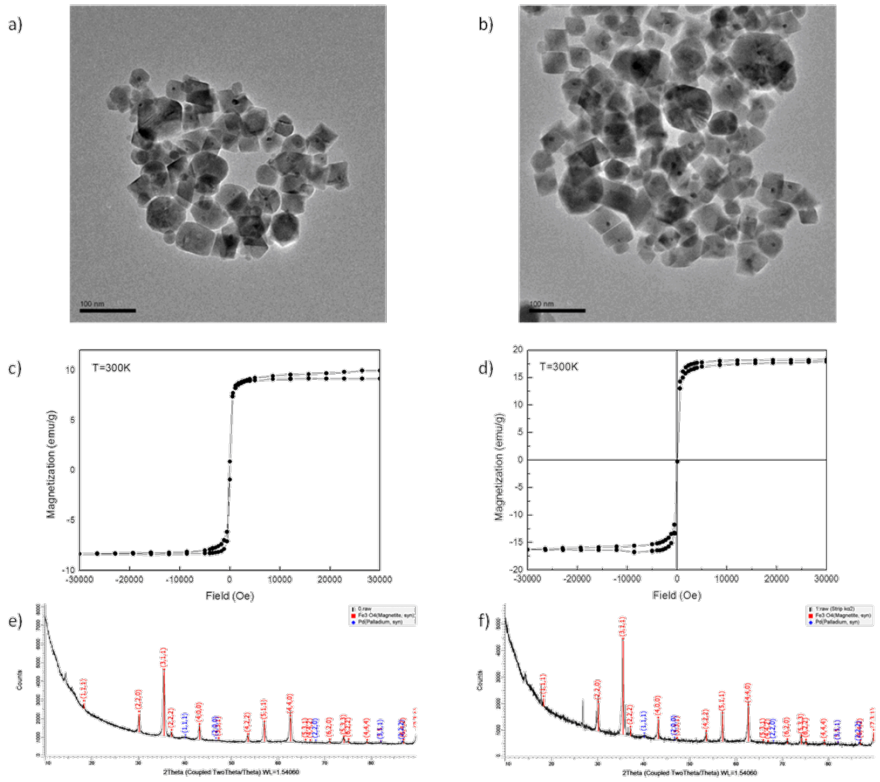

Figure 3. Characterization data of heterodimeric nanoparticles before use (left) and after recycling (right): (a) and (b), TEM images; (c) and (d), magnetic behavior; (e) and (f), XRD patterns.

These several outcomes suggested the mechanism of Pd-Fe_3O_4 nanocrystals that the nanocrystal was preserved during the catalytic cycle. But evidences against our proposed mechanism were observed in further reaction screening progress and they exhibited the possibility that a reaction was catalyzed by leached Pd species. So we designed and carried out experiment to identify the mechanistic aspects of Pd-Fe_3O_4 nanocrystals.

To determine the true catalysts for reactions, Suzuki reactions using polymer resin were carried out. A polymer-bound resin, 2-mercaptoethylamine (Aldrich No. 641022), was used as transition metal scavenger and it is expected to capture the palladium in solution. Same

reactions with homogeneous palladium source ($Pd(OAc)_2$) and Pd-Fe_3O_4 nanocrystal were carried out. As a result, it was found that Pd-Fe_3O_4 nanocrystals lost their reactivity with scavenger just as homogeneous palladium catalysts. This phenomenon suggests us that the catalysis reactions are carried out by dissolved palladium from nanocrystals.

To further interrogate the leaching out phenomenon, we have carried out a series of tests including "hot filtration" test.[18] For hot filtration test in Wacker oxidation and Heck reaction, Pd-Fe_3O_4 nanocrystals were collected at the bottom of the flask by a neodymium magnet, and the supernatant solution was separated while the solution is hot. During the process, the temperature is maintained through the process. The catalytic activity of the separated solution was then tested. If there is conversion of the remaining substrate to products, the converted amount is measured through gas chromatographic analysis. If the reaction takes place only at the surface of nanocrystals, the supernatant solution would not show any catalytic activity. Conversely, if there is any catalytic palladium released from the nanocrystals remains in the solution phase, then the catalytic activity would also appear in the separated solution. As a result, 20% additional conversion was observed in the Wacker oxidation. In the case of Heck reaction, there was just 5% additional conversion. The difference between the two reactions is apparently due to the difference of the leached Pd amount under the different reaction conditions and in the Wacker oxidation more palladium is released from nanocrystals and the conversion ratio is increased. In the hot filtration test, additional conversion observed in the solution phase suggests that catalysis is carried out by dissolved palladium that has leached into solution from nanocrystals.

We investigated the reaction rate of the Pd-Fe_3O_4 nanocrystals toward the Suzuki coupling reaction and compared them with that of homogeneous $Pd(OAc)_2$. The substrate and product distribution was measured by GC

analysis. As shown in figure 4, a time lag was observed in the reaction using the Pd-Fe_3O_4 nanocrystals. This observation strongly suggests that, catalysis using the Pd-Fe_3O_4 needs a time to generate a "true" catalyst species in the homogeneous phase.[19] The soluble palladium species is considered to dissolve out from the nanocrystals at elevated reaction temperature.

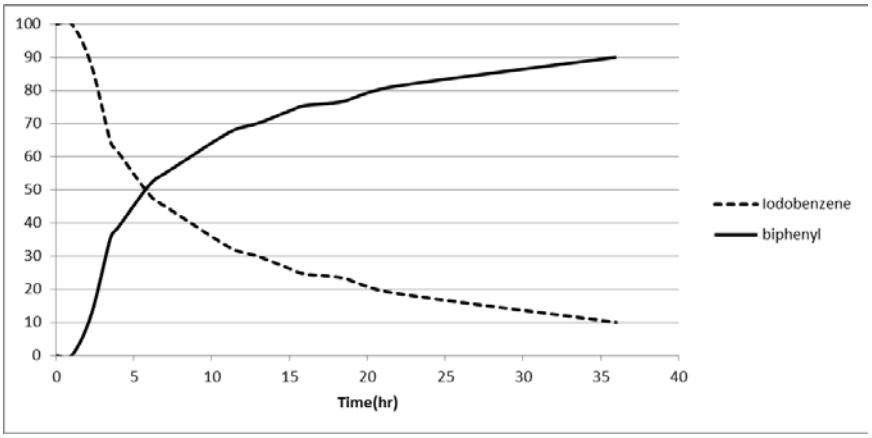

Figure 4. Reactions rates of the Pd-Fe3O4 toward the Suzuki coupling reaction

Several other experiments also suggest that there is similar evidence for the mechanism of Pd-Fe_3O_4 nanocrystals. It is considered that the reactions occur in homogeneous phase by soluble palladium from Pd-Fe_3O_4 nanocrystals.

3. Conclusion

In summary, we demonstrated catalytic applications of Pd-Fe_3O_4 heterodimeric nanocrystals as magnetically separable catalysts. These heterodimeric nanocrystals are simply prepared in gram-scale by a two-step sequential heating of a mixture of $Fe(acac)_3$ and $Pd(acac)_2$. We successfully applied the nanocrystals as catalysts, in the absence of additive ligands, to

various organic reactions such as Suzuki, Heck, and Sonogashira coupling reactions, as well as direct C-H arylation. Such Pd-Fe_3O_4 heterodimeric nanocrystal catalyst system has several advantages over conventional homogeneous and heterogeneous systems, including good activity, reusability and atom efficiency. In this catalysts system, the amount of leached palladium is quite small and the shape of nanocrystals is maintained during the reactions. After reactions, the nanocrystal catalyst could be easily separated from the mixture through the use of a magnet and could be recycled several times without losing catalytic activity. Furthermore, almost 100 times less Pd was found in the products compared to that obtained from the analogous homogeneous reaction. This recyclable and ligand-free nanocrystal catalyst system provides efficient and eco-friendly synthetic methods for palladium-catalyzed reactions. Therefore, the Pd-Fe_3O_4 heterodimeric nanocrystals have a great potential for the development of greener synthetic methods for a wide range of applications that are not only restricted to laboratory but also large scale preparations amenable to bulk chemical and pharmaceutical industry.

4. Experimental

General experimental

Without additional notes, all reagents were commercially available and used without further purification. Oleic acid and oleylamine were purchased from Aldrich Chemical Co. Iron(III) acetylacetonate ($Fe(acac)_3$, 99%) was purchased from Acros. Palladium(II) acetylacetonate ($Pd(acac)_2$, 99%) was purchased from Strem. THF was distilled over sodium and benzophenone, and degassed by argon bubbling for 10 minutes before using on polymerization. Toluene, 1,4-dioxane, methanol and DMF were purified by solvent purification system using alumina column, and degassed by argon bubbling.

N,*N*'-Dimethylacetamide (DMA) was purchased from Junsei and degassed through argon bubbling for 10 minutes before using on polymerization without further purification.

Sonication was carried out in a 120 W ultrasonic bath (Branson, B-3210). Flash column chromatography was performed on silica gel with eluents of a mixture of hexane and ethyl acetate. ^{1}H and ^{13}C NMR spectra were obtained on Agilent MR DD2 (400 MHz) spectrophotometer.

All transmission electron microscopy (TEM) and high-resolution TEM (HRTEM) images were obtained on a JEOL EM-2010microscope at an accelerating voltage of 200 kV. The powder X-ray diffraction (XRD) was performed using a RigakuD/Max-3C diffractometer (CuKa radiation, l = 0.15418 nm). The magnetic properties were characterized using a vibrating sample magnetometer (Quantum Design PPMS VSM) at 300 K. Thermogravimetric analysis (TGA) was carried out on a thermal analyzer (Perkin Elmer TAC 7/DX) at a heating rate of 10 ^{o}C/min under nitrogen atmosphere. Fourier transform infrared (FT-IR) spectra were obtained on a PerkinElmer Spectrum One FT-IR spectrophotometer using KBr pellets. Inductively coupled plasma mass spectrometry (ICP-MS) was performed by using ICPS-7500 spectrometer (Shimadzu).

GC analyses were performed on HP-6890 series with HP-5 capillary column (30 m x 0.25 mm; coating thickness 0.25 μm). Gas chromatography-mass spectroscopy (GC-MS) was performed with 5973N mass selective detector (Agilent) and HP-5MS column.

Preparation of Pd-Fe_3O_4 heterodimeric nanocrystals

The synthesis of Pd-Fe_3O_4 was performed by two-step thermal decomposition of a mixture composed of iron acetate, palladium acetate, oleylamine, and oleic acid. In a typical experiment, 200mg of $Pd(acac)_2$ (0.66

mmol) and 14 g of $Fe(acac)_3$ (40 mmol) were added into a solution containing 120 mL of oleylamine (350 mmol) and 80 mL of oleic acid (250 mmol), and the mixture was heated to 120 ^oC under reduced pressure with vigorous stirring for 2 h. The resulting dark brown solution was heated to 220 ^oC under Ar atmosphere at a heating rate of 2 ^oC/min and the mixture was kept at this temperature for 30 min, and then it was further heated to 300 ^oC at the same heating rate and aged for 30min. After cooled to ambient temperature, the reaction mixture was treated with 250 mL of ethanol to induce precipitation, and the resultant powdery nanocrystals were retrieved by centrifugation (1700 rpm, 15 min). The nanocrystals were purified by dispersing in 150 mL of hexanes and collected with a neodymium magnet (3880 G, 50 mm diameter, 10 mm thick). These washing cycles were repeated until the hexane layer showed no color, at which point the Pd-Fe_3O_4 nanocrystals were dried under vacuum (2.8 g).

We performed several kinds of control experiments to optimize the reaction conditions and to understand the formation mechanism. When $Pd(acac)_2$ was solely used as the precursor, severely aggregated Pd nanoparticles were generated presumably due to the weak binding of oleylamine to the surface of Pd nanoparticles. On the other hand, when $Fe(acac)_3$ was thermally decomposed, uniform 14 nm-sized spherical iron oxide nanocrystals were produced, as reported by Sun and co-workers. We optimized the synthesis conditions by varying heating temperatures and heating rates. It was found that the Pd–Fe_3O_4 heterodimer nanocrystals were produced under only optimized conditions. When the synthesis was conducted under other conditions, mixtures of the Pd–Fe_3O_4 heterodimer nanocrystals and Fe_3O_4 nanocrystals were generated. Furthermore, the two-step heating process turned out to be critical for the synthesis of the Pd–Fe_3O_4 heterodimer

nanocrystals. When the aging step at 220 ^{o}C was skipped, a mixture of Fe_3O_4 nanocrystals and Pd nanocrystals was generated. The sequential heating method is similar to that used in the synthesis of Ni/Pd core/shell nanocrystals from consecutive thermal decomposition of Ni–TOP (trioctylphosphine) and Pd–TOP complexes.[20] The optimal aging is also important for the formation of Pd–Fe_3O_4 heterodimer nanocrystals. When the aging time at 220 ^{o}C was increased to 1 h, a mixture of Fe_3O_4 nanocrystals and Pd nanocrystals was produced.

To understand the formation mechanism, we took aliquot samples and analyzed them with TEM at various stages during the synthesis. At 200 ^{o}C, only Pd nanoparticles were produced and no formation of Fe_3O_4 particles was observed. As the reaction temperature is increased, Fe_3O_4 particles progressively grew on the as-synthesized Pd nanoparticles. At 220 ^{o}C, Fe_3O_4 nanoparticles began to form on the surface of Pd nanoparticles. The growth of Fe_3O_4 nanoparticles on the surface of Pd nanoparticles proceeded until the temperature reached 300 ^{o}C. These results clearly showed that the initially formed Pd nanoparticles act as seeds for the heterogeneous nucleation of the iron oxide nanoparticle to produce the Pd–Fe_3O_4 heterodimer nanocrystals. To verify the suggested mechanism of heterodimer formation, we prepared Pd nanoparticles in the TOP coordinating solvent separately and 10 mg of Pd nanoparticles were added into the mixture solution containing 0.14 g of $Fe(acac)_3$, 6 mL of oleylamine, and 4 mL of oleic acid. The mixture was heated to 300 ^{o}C and the product is almost the same as the one-pot synthesized heterodimers that we described. The experimental result is also supported by the previous work by Teranishi and his coworkers, which reported that Pd/γ-Fe_2O_3 heterostructured nanoparticles could be synthesized by Pd-seed-mediated synthesis.[21]

The formation of heterodimers, not core–shell particles, can be explained from the electron density of seeds. Zeng and Sun described that the structure of nanoparticles (core–shell or heterodimer) is determined by the polarity of the solvent. When a nonpolar solvent is used, a nucleation site of seed nanoparticles depletes the electrons from nanoparticles and the electron deficiency cannot be replenished from the solvent, resulting in the formation of heterodimer nanoparticles. On the other hand, the polar solvent tends to donate electrons to seed nanoparticles with electron deficiency. Accepting the electrons from the solvent causes the increase of nucleation sites on seeds, resulting in the formation of core-shell nanoparticles. In our one-pot synthetic procedure, electrons of the solvent were consumed to synthesize Pd nanoparticles and were not provided to seed Pd nanoparticles, resulting in the formation of heterodimer nanocrystals, not core–shell particles.

Characterization of Pd-Fe_3O_4 heterodimeric nanocrystals

The TEM images of the products showed that nearly all of the heterodimer nanocrystals are composed of a single Pd nanosphere with a diameter of ~6 nm and a faceted Fe_3O_4 nanocrystal with a dimension of ~30 nm. A high resolution TEM (HRTEM) image clearly showed the (111) planes of the Pd component with a d-spacing of 0.22 nm and the (220) planes of the Fe_3O_4component with a d-spacing of 0.296 nm. The heterodimeric shape of the Pd–Fe_3O_4 nanocrystals was confirmed by changing the tilted angle (X1) during the TEM measurement, which clearly showed that the Pd nanosphere is directly attached on the Fe_3O_4 nanocrystal. All peaks of the X-ray diffraction (XRD) pattern (Fig. 1c)can be assigned to the (111), (200), (220), (311), and(222) lattice planes of a face-centered cubic (fcc) Pd crystal structure (JPCDS 46-1043) and the (220), (311), (400),(422), (511), (440), and (533) lattice planes of fcc Fe_3O_4(JCPDS 88-0315). The ED pattern also

confirmed that the nanocrystals were composed of fcc Fe_3O_4 and fcc Pd. The magnetic properties of the heterodimer nanocrystals were characterized using a vibrating sample magnetometer (VSM) at 300 K. The hysteresis loop in the M–H curve at 300 K revealed that the nanocrystals were soft ferromagnetic with a saturation magnetization value and a low coercivity value. The nanocrystals are suitable for magnetic separation applications.

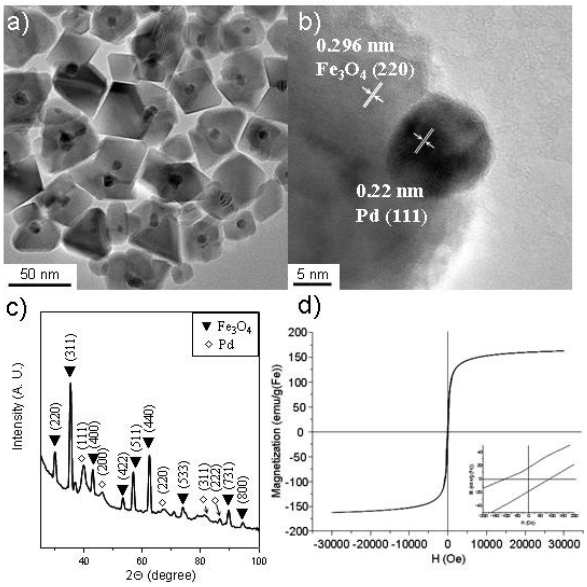

General procedure for Suzuki coupling

Degassed solvent (1,2-dimethoxyethane:H_2O=3:1 or 1,4-dioxane), aryl halide (1.0 mmol), aryl boronic acid (1.2 mmol), base (1.3 mmol), and the nanocrystal catalyst (1.0 mol%) were added to a round-bottom flask, which was backfilled with argon. The reaction mixture was refluxed for 24 h with vigorous stirring. After the reaction, the reaction mixture was cooled to room temperature and the catalyst was separated using a magnet. The mixture containing products was extracted with methylene chloride and water, the organic layer was concentrated and purified through flash chromatography using hexane and ethyl acetate (20:1 v/v) as an eluent.

General procedure for Heck reaction

Degassed solvent (DMF), aryl halide (1.0 mmol), olefin (1.0 mmol), base (1.5 mmol), and the nanocrystal catalyst (1.0 mol %) were added to a round-bottom flask, which was backfilled with argon. The reaction mixture was stirred for 24 h at 110 ^{o}C. After the reaction, the mixture was cooled to room temperature and the catalyst was separated using a magnet. The mixture containing products was partitioned between methylene chloride and water and organic layer was concentrated and purified through flash chromatography using hexane and ethyl acetate (20:1 v/v) as an eluent.

General procedure for Sonogashira reaction

Degassed solvent (DMF), aryl halide (1.0 mmol), phenyl acetylene (1.0 mmol), base (1.5 mmol), and the nanocrystal catalyst (1.0 mol %) were added to a round-bottom flask, which was backfilled with argon. The reaction mixture was stirred for 24 h at 110 ^{o}C. After the reaction, the mixture was cooled to room temperature and the catalyst was separated using a magnet. The mixture containing products was partitioned between methylene chloride and water, and the organic layer was concentrated and purified through flash chromatography using hexane and ethyl acetate (20:1 v/v) as an eluent.

General procedure for C-H arylation

Degassed solvent (DMA, 2 mL) were dissolved aryl bromide (0.5 mmol), imidazo[1,2-a]pyridine(0.75 mmol), NaOAc (1.0 mmol), and the nanocrystal catalyst (1.0 mol %). The resulting suspension was degassed by argon for 10 min, sonicated for 3 min, and stirred at 166 ^{o}C for 12 h. After cooled to room temperature, the reaction mixture was filtered with a short silica gel pad and concentrated under reduced pressure. Alternatively, the reaction mixture was concentrated after magnetic separation of Pd-Fe_3O_4. The crude product was

purified by flash column chromatography on a silica gel column.

Chapter 2. Selective semihydrogenation of alkynes on shape-controlled palladium nanocrystals

1. Introduction

Selective semihydrogenation of alkynes to alkenes is of great importance in the production of olefins in relation to the synthesis of natural products and fine chemicals.[1] Palladium is one of the most widely used catalysts for hydrogenation reactions,[2] but it usually exhibits low alkene selectivity in alkyne hydrogenation due to its high efficiency in promoting the addition of hydrogen to carbon-carbon double bonds, which leads to further reduction into alkanes. Traditionally, use of the Lindlar catalyst, which consists of deactivated palladium supported on $CaCO_3$ or $BaCO_3$, has been the method of choice for semihydrogenation of alkynes owing to its high alkene selectivity, although Pd/C catalysts have also been employed.[3-5] The Lindlar catalysts are usually poisoned by a lead complex, with quinoline as an additional poison, for the enhancement of the alkene selectivity. This makes the Lindlar catalysts often suffer from the production of harmful wastes due to the incorporation of toxic additives.[5]

The catalytic properties of metal nanocrystals can be drastically enhanced by the control of their shapes, which determine surface atomic arrangements and thus affect activity and/or selectivity toward a specific catalytic reaction.[6] Here we demonstrate that in the alkyne hydrogenation, high alkene selectivity can be achieved simply by shaping Pd nanocrystals to expose facets that favor the adsorption of alkyne. In this work, we synthesized Pd nanocrystals with a cubic shape and thus exposed {100} facets and then applied them to selective semihydrogenation of various alkynes including 5-decyne, 2-butyne-1,4-diol, and phenyl acetylene. For all substrates, the Pd nanocubes exhibited higher alkene selectivity (>90%) as compared to commercial Pd/C catalyst (75~90%). Our results show great promise toward developing a highly efficient and reliable catalyst for selective semihydrogenation of alkynes without employing toxic additives.

2. Results and Discussion

Palladium nanocubes were synthesized using a previously reported method.[7] A typical transmission electron microscopy (TEM) image of the as-prepared Pd nanocrystals showed the formation of nanocubes as a major product in addition to a small portion of nanobars that were slightly elongated along one direction (Figure 5a). They exhibit an average edge length of approximately 11 nm (Figure 5b). The powder X-ray diffraction (XRD) pattern in Figure 1c shows that the Pd nanocubes have a face-centered cubic (fcc) structure (Fm3m, a = 3.958 Å, JCPDS Card No. 87-0641). The six faces of a Pd nanocube are bounded by {100} facets, as revealed by the high-resolution TEM (HRTEM) image and an array of spots with square symmetry in the corresponding Fourier-transform (FT) pattern in Figure 5d.

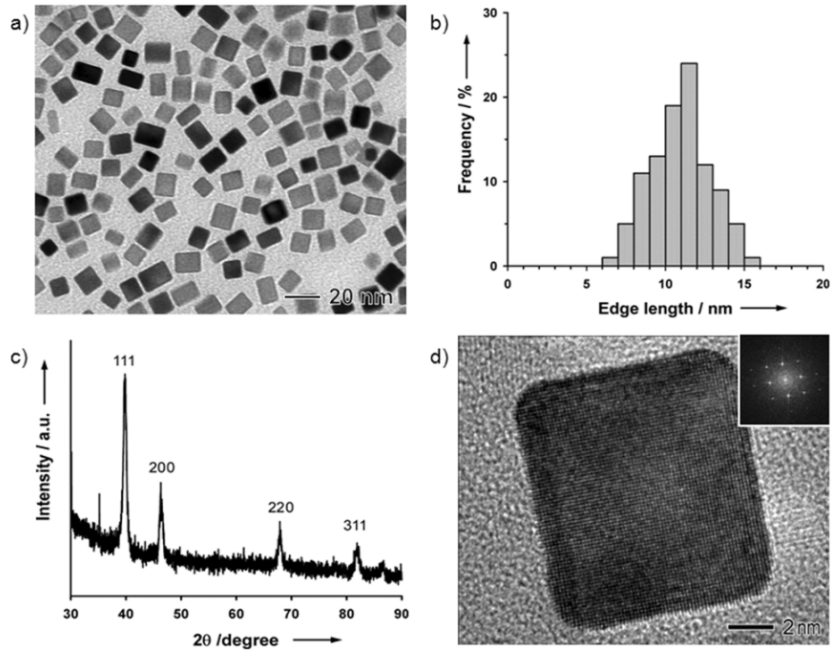

Figure 5.Characterization of Pd nanocubes. a) TEM image, b) particle size, and c) powder XRD pattern. d) HRTEM image of a single Pd nanocube shown in (a) and the corresponding FT pattern (inset).

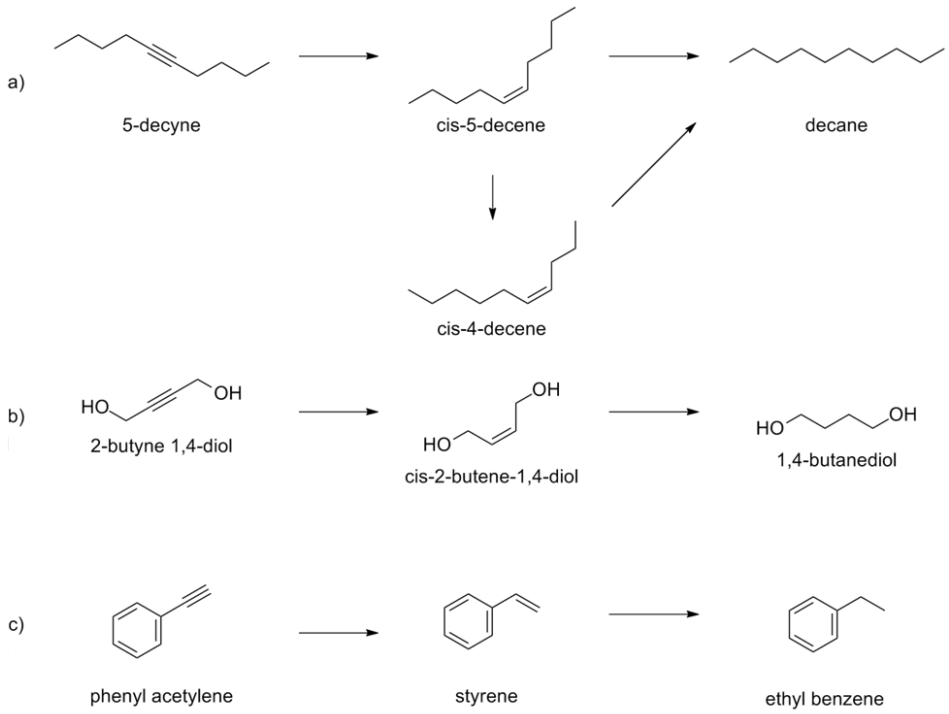

Scheme 3. Reaction pathways for the hydrogenation of a) 5-decyne, b) 2-butyne-1,4-diol, and c) phenyl acetylene.

We first investigated the catalytic properties of the Pd nanocubes toward the hydrogenation of 5-decyne (Scheme 3a) against those of commercial Pd/C catalyst (10% by weight of ca. 3-nm Pd nanoparticles on activated carbon support) (Figure 6). The hydrogenation reactions of 5-decyne were conducted at room temperature under 1 atm hydrogen pressure with initial sample concentrations of about 0.20 M in ethanol and 1.0 mol% of the Pd nanocubes or commercial Pd/C catalyst. The reactant and product distribution was evaluated through gas chromatography (GC) analysis. When the reaction was catalyzed by the Pd nanocubes, high selectivity (95%) to cis-5-decene was observed at ~98% conversion of 5-decyne (Table 1). After full conversion of 5-decyne, 5-decene was readily overhydrogenated to decane (Figure 7a), indicating that the {100} facets on the Pd nanocubes also catalyzed the hydrogenation of 5-decene effectively. It is worth noting that the

semihydrogenation and the overhydrogenation stages are well separated, as shown in Figure 7a. In the case of the commercial Pd/C catalyst, however, semihydrogenation was accompanied by significant overhydrogenation even at low conversion stages of 5-decyne (Figure 7b), resulting in the formation of a 75/20 mixture of 5-decene/decane at ~95% conversion of 5-decyne (Table 11). This observation clearly indicates the higher alkene selectivity of the Pd nanocubes for the semihydrogenation of 5-decyne as compared to the commercial Pd/C catalyst.

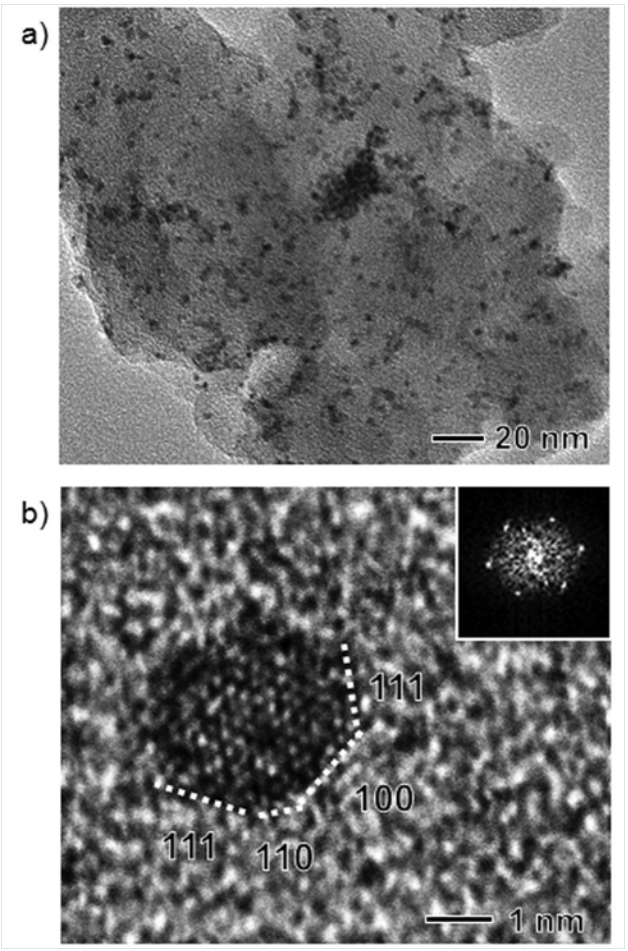

Figure 6. a) TEM image of the commercial Pd/C catalyst. b) HRTEM image of a single Pd nanocrystal in (a). The inset shows the corresponding FT pattern.

Table 11. Product distribution in the hydrogenation of alkynes.[a]

Substrate	Catalyst	Product distribution [%][b]	
		cis-Alkene[c]	Alkane
5-decyne	Pd	95	3
	Pd/C	75	20
2-butyne-1,4-diol	Pd	98	2
	Pd/C	88	11
phenyl acetylene	Pd	91	9
	Pd/C	80	19

[a] Reaction conditions: (substrate 0.20 M) in ethanol and 1.0 mol% of a catalyst at room temperature and 1 bar hydrogen pressure. [b] All the products were identified by comparison with authentic samples using GC analysis. [c] Formation of *trans*-alkene was not detected on GC analysis.

We also carried out hydrogenation of 2-butyne-1,4-diol and phenyl acetylene (Scheme 3, b and c). At full conversion, the Pd nanocubes exhibited high alkene selectivities of 98 and 91% for the semihydrogenation of 2-butyne-1,4-diol and phenyl acetylene, respectively, (Table 11 and Figure 7, c and e). On the contrary, the commercial Pd/C catalyst resulted in the formation of an 88/11 mixture of 2-butene-1,4-diol/butane-1,4-diol at a full conversion of 2-butyne-1,4-diol and an 80/19 mixture of styrene/ethylbenzene at a 99% conversion of phenyl acetylene (Table 11 and Figure 7, d and f). These results suggest that the Pd nanocubes could be applied as a highly selective catalyst for the semihydrogenation of various alkynes.

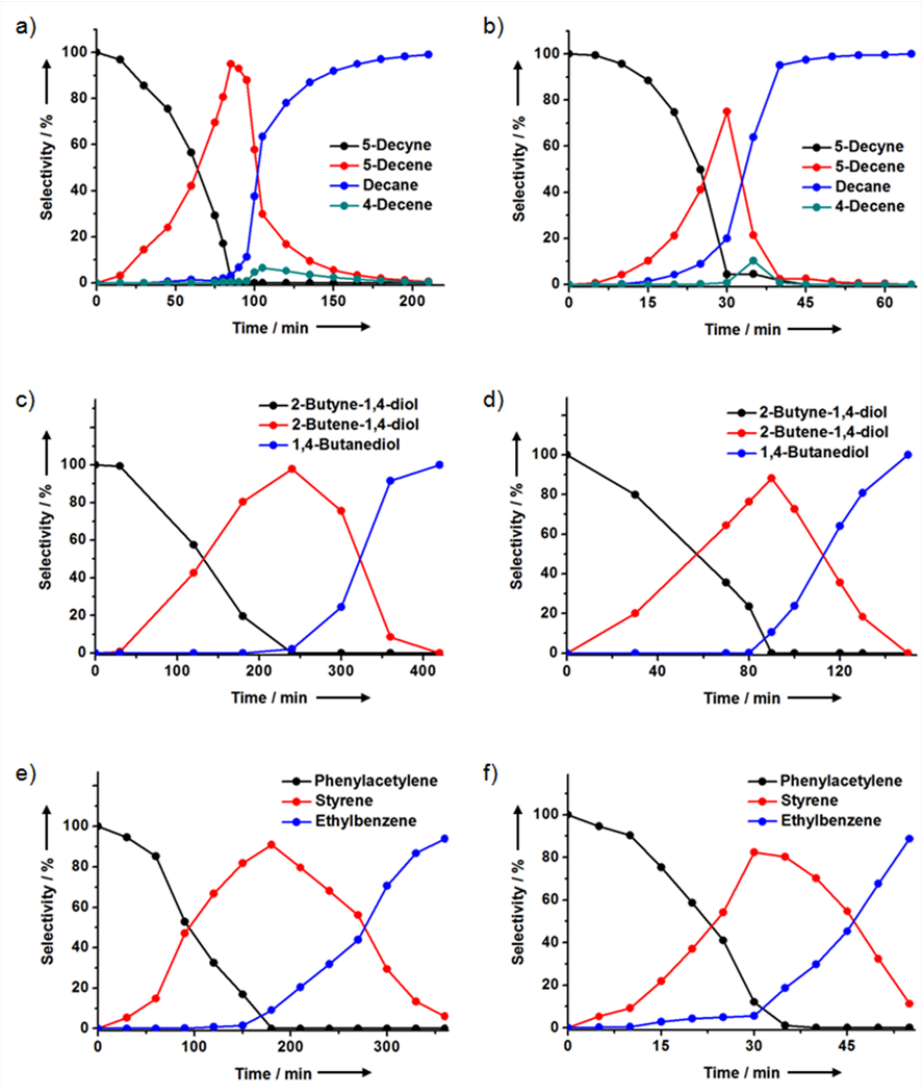

Figure 7. Hydrogenation of various alkynes on a, c, e) Pd nanocubes and b, d, f) commercial Pd/C catalyst: a, b) 5-decyne; c, d) 2-butyne-1,4-diol; and e, f) phenyl acetylene

Then we investigated the effect of the catalyst concentration on the product distribution in the hydrogenation of 5-decyne. Higher alkene selectivities were still observed from the reactions using the Pd nanocubes in a wide range of concentrations from 0.5 to 2.0 mol%, but reactions with the Pd/C catalyst showed lower alkene selectivity at the same range of concentrations (Figure 8). This result illustrates that higher alkene selectivity of the Pd nanocubes in

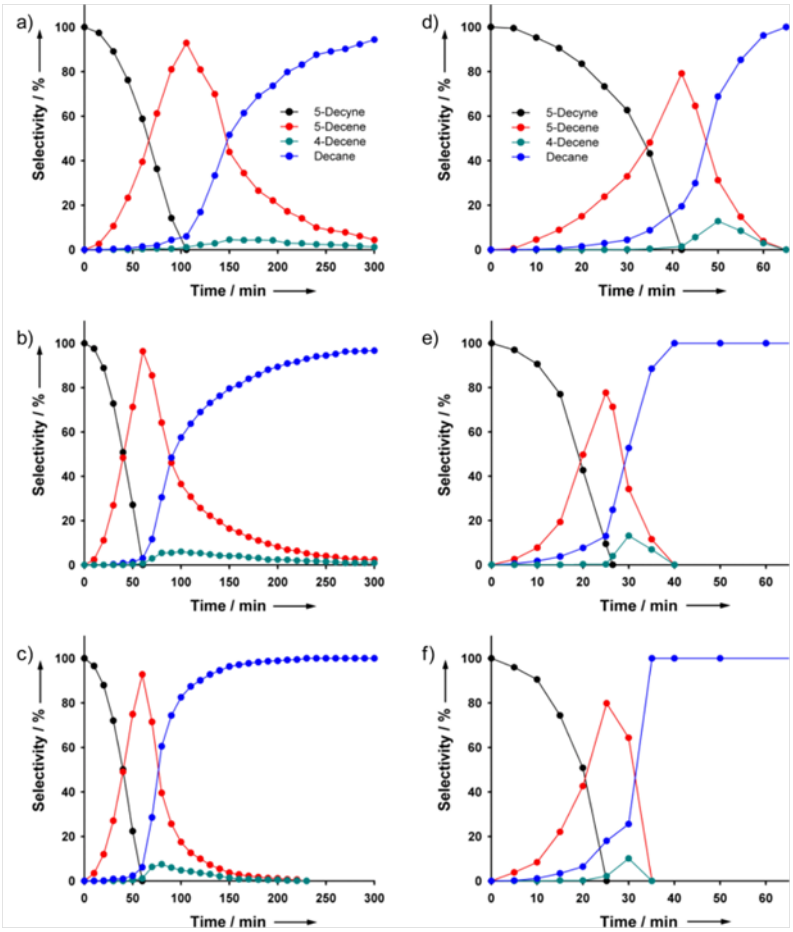

Figure 8. Hydrogenation of 5-decyne on a) 0.5 mol% Pd nanocubes, b) 1.5 mol% Pd nanocubes, c) 2.0 mol% Pd nanocubes, d) 0.5 mol% Pd/C, e) 1.5 mol% Pd/C, and f) 2.0 mol% Pd/C

the semihydrogenation of alkynes was enabled by their shape rather than the catalyst concentration, thus chemoselective reduction of alkynes by use of shape-controlled Pd nanocrystals is practically a viable process.

Representative TEM images of the Pd nanocubes obtained after the hydrogenation of 5-decyne confirmed their morphological stability (Figure 9), strongly suggesting that the nanocrystal shape was indeed responsible for the observed catalytic behavior. Inductively coupled plasma atomic emission

spectroscopy (ICP-AES) analysis revealed that the Pd nanocubes did not show any apparent leaching of Pd into the solution during the reaction. The as-synthesized Pd nanocubes may contain residual bromide ions adsorbed on their surface. The X-ray photoelectron spectroscopy (XPS) analysis of the Pd nanocubes revealed the presence of bromine signals even after extensive washing of the nanocubes with ethanol and water (Figure 10), which implies that it is very difficult to completely remove bromide ions from the nanocube surface. We investigated to see if bromide ions adsorbed on the surface of Pd nanoparticles affect their catalytic behavior. The hydrogenation of 5-decyne was carried out with the Pd/C catalyst that had been pre-treated with KBr, and we did not observed any noticeable change in the catalytic behavior of the Pd/C catalyst before and after the treatment with bromide ions (Figure 11). Our results suggest that bromide ions adsorbed on the particle surface do not have a significant effect on the catalytic behavior of a given catalyst in the alkyne hydrogenation.

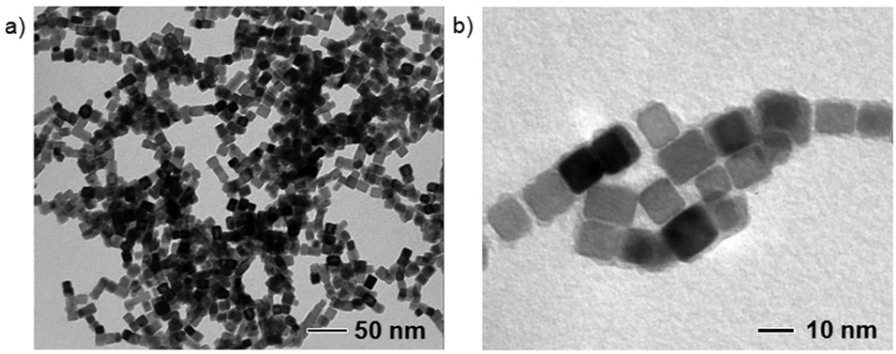

Figure 9. TEM images of Pd nanocubes obtained after the hydrogenation of 5-decyne

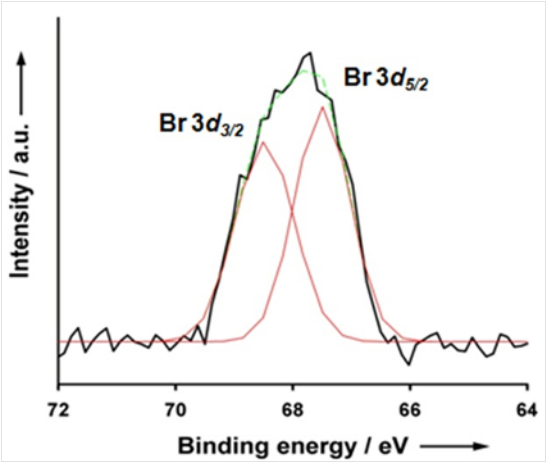

Figure 10. Br 3d XPS core level spectrum taken from the Pd nanocubes after extensive washing with ethanol and water. In the spectrum, the Br $3d_{5/2}$ and Br $3d_{3/2}$ binding energies were 67.6 and 68.5 eV, respectively, which were close to the literature values for Br^-.[9]

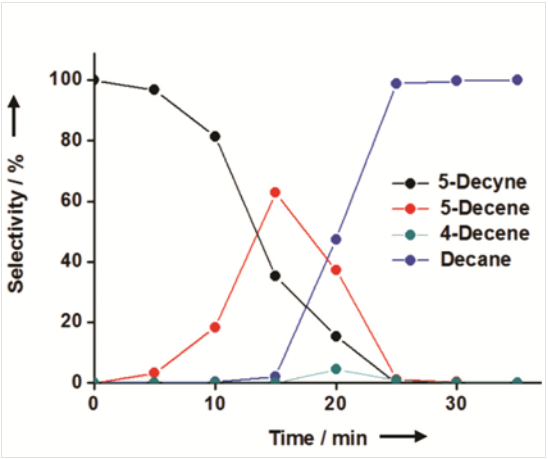

Figure 11. Hydrogenation of 5-decyne on 2.0 mol% Pd/C catalyst that were pre-treated by bromide ions. The pre-treatment was conducted by heating 11 mL of an aqueous mixture containing the commercial Pd/C catalyst (200 mg) and KBr (200 mg) at 80 ^oC for 3 h.

We propose that the higher alkene selectivity of the Pd nanocubes may arise from a large difference in the adsorption energies of alkynes and alkenes on their surface. In hydrogenation, the adsorption strengths of substrates on a given metal surface are known to increase on the order of alkane < alkene <

alkyne.[8] To investigate the surface structure-sensitive adsorption of alkyne and alkene, we performed density functional theory (DFT) calculations taking acetylene and ethylene as model molecules. Figure 12 illustrates lowest energy states for the adsorption of acetylene and ethylene on Pd(100) and Pd(111), respectively. The DFT calculations revealed that on Pd(100), the adsorption energy of acetylene (-2.61 eV) is much stronger than that of ethylene (-0.96 eV) (Table 12). Furthermore, the difference in binding energies between acetylene and ethylene was larger on Pd(100) (ΔE = 1.65 eV) than on Pd(111) (ΔE = 1.13 eV), suggesting that Pd(100) is better suited for the selective binding of acetylene than Pd(111). The Pd nanocubes would favor the adsorption of alkynes owing to the predominant exposure of {100} facets on their surfaces. During the semihydrogenation, unreacted alkynes could readily substitute freshly formed alkenes on the {100} facets of the Pd nanocubes and thus impede the overhydrogenation into alkanes, which apparently contributes to the high alkene selectivity. Once alkynes have been consumed, alkenes could be adsorbed on the {100} facets of the Pd nanocubes and then be hydrogenated to alkanes, as demonstrated in Figure 7. Meanwhile, small Pd nanoparticles on the Pd/C catalyst take a truncated octahedral shape, whose surface is bound by a mix of {100} and {111} facets (Figure 6b). This shape also contains a large fraction of edge atoms, which serve as active sites not only for the semihydrogenation but also for the overhydrogenation due to increased adsorption strength of alkenes[9] and thus lower the overall alkene selectivity.

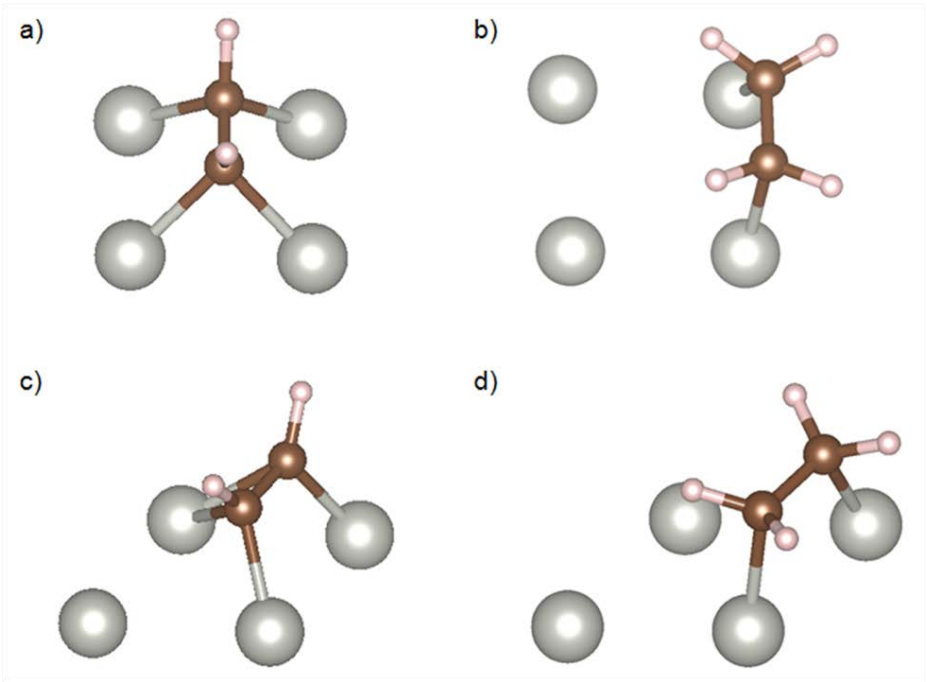

Figure 12. Illustrations of the lowest energy adsorption modes of acetylene and ethylene on Pd(100) and Pd(111): a) acetylene on a 4-fold hollow site of Pd(100); b) ethylene on a 2-fold aligned bridge site of Pd(100); c) acetylene on a 3-fold hcp site of Pd(111); and d) ethylene on a 2-fold aligned bridge site of Pd(111).

Table 12. Adsorption energies of acetylene and ethylene on Pd(100) and Pd(111) surfaces.

Substrate	Pd surface	Adsorption energy(eV)
Acetylene	(100)	-2.61
	(111)	-2.01
Ethylene	(100)	-0.96
	(111)	-0.88

Table 13. Selective hydrogenation of alkynes using Pd nanocubes.[a]

Entry	Substrate	Reaction time	Product distribution (%)		
			cis-Alkene	*trans*-Alkene	Alkane
1	1-octyne	80 min	85.7	0.0	8.6
2	1-decyne	90 min	81.9	0.0	12.7
3	2-decyne	90 min	84.4[a]	0.0	7.3
4	3-decyne	90 min	85.2[a]	0.0	6.6
5	4-decyne	80 min	89.3[a]	0.0	7.8
6[b]	5-decyne	10 h	93.6	0.0	0.2
7[c]	5-decyne	18 h	93.2	4.9	0.0

[a] Reaction conditions: substrate (0.20 M) and 1.0 mol% of catalyst in ethanol were stirred at room temperature under 1 atm hydrogen pressure. [b] The reaction was carried out at 0°C. [c] The Lindlar catalyst (1 mol%, Acros) was used instead of Pd nanocubes.

We have also carried out hydrogenation of several internal and terminal alkynes using the Pd nanocubes as catalysts. As summarized in Table 13, hydrogenation reactions using the Pd nanocubes exhibited extremely high *cis*-alkene selectivities regardless of the location of the triple bond in alkynes. In all the cases examined in the reduction of internal alkynes with the Pd nanocubes, no trace of trans-alkene was detected as product (Table 13, entries 3-6). Moreover, overhydrogenation to alkane could be suppressed almost completely by lowering the reaction temperature to 0 °C (Table 13, entry 6). For comparison, reduction of 5-decyne to 5-decene was carried out employing 1.0 mol% Lindlar catalyst and after 18 h a mixture of products was obtained consisting of 93.2% *cis*-decene and 4.9% *trans*-decene (Table 13, entry 7). The Lindlar catalyst has been known to be very efficient for the semihydrogenation of alkynes to cis-alkenes, but reactions using the Lindlar catalyst are reported to often suffer from Z/E isomerization, low reactivity and poor reproducibility.[11] On the contrary, the reactions employing Pd nanocubes consistently showed higher reactivity and much more enhanced cis-alkene

selectivity than those with the Lindlar catalyst. Furthermore, Pd nanocubes could be easily recovered by filtration and offers a very convenient way to recycle the catalyst.

3. Conclusion

In summary, we have studied the alkyne hydrogenation on shape-controlled Pd nanocrystals enclosed by {100} facets. The Pd nanocubes exhibited higher alkene selectivity in the semihydrogenation of various alkynes including 5-decyne, 2-butyne-1,4-diol, and phenyl acetylene than the commercial Pd/C catalyst, which was enabled by predominant exposure of {100} facets on their surface. The Pd nanocubes also presented superior cis-selectivity to the traditional Lindlar catalyst in the reduction of internal alkynes. Our results demonstrate that shape control of Pd nanocrystals provides a simple and efficient way for generating highly selective catalysts for the alkyne semihydrogenation. The shape-controlled Pd nanocrystals reported herein could serve as attractive candidates for the fundamental study of nanocrystal shape effect on various Pd-based catalytic reactions.

4. Experimental

General experimental

Lindlar catalyst (5 wt% Palladium on calcium carbonate; poisoned with lead) was purchased from Acros organics(C.A.S 7440-05-3) and Pd/C(Palladium, 10 wt% on activated carbon, Degussa type) was purchased from Aldrich(Catalog No.330108). All the rest commercial materials were purchased from Aldrich Chemical Co or Tokyo Chemical Industry Co and were used without further purification.

TEM studies were done with a LIBRA 120 (Carl Zeiss) microscope operated at 120 kV by drop casting the dispersions of nanoparticles on carbon-coated copper grids. HRTEM analyses were performed using a JEOL 2100F operated at 200 kV accelerating voltage. Powder XRD measurements were conducted using an M18XHF-SRA (Mac Science) diffractometer equipped with a CuKa radiation source (λ = 1.5406 Å) at 40 kV and 300 mA (12 kW). GC analyses were performed with a HP-6980 series chromatograph with HP-5 capillary column (30 m x 0.25 mm; coating thickness 0.25 μm).

Synthesis of Pd nanocubes

In a typical synthesis of Pd nanocubes, 11 mL of an aqueous solution containing poly(vinylpyrrolidone) (PVP, MW = 55,000, 105 mg, Aldrich), L-ascorbic acid (60 mg, Aldrich), KBr (200 mg, Aldrich), and Na_2PdCl_4 (57 mg, Aldrich) was heated at 80°C in air under magnetic stirring for 3 h and cooled down to room temperature.

General procedure for Alkyne Hydrogenation

Pd catalyst and degassed ethanol (2.0 mL) were added into a 5 mL round-bottom flask, and the mixture was sonicated in an ultrasonic bath for 10 minutes. After sonication, substrate (0.40 mmol) was added to the flask and the mixture was stirred at room temperature under a hydrogen balloon. The course of the reaction was periodically followed by taking aliquots (10 μL) and then analyzing them using Hewlett Packard 5890 Gas Chromatography (GC).

DFT calculations

First principles calculations were performed to estimate the adsorption energies of acetylene and ethylene on Pd surface using the Vienna Ab Initio

Simulation Package (VASP).[10,11] In the calculations, the molecules are adsorbed on a Pd slab, which has a periodic 2 × 2 unit cell with 4 and 5 layers for (100) and (111) surfaces, respectively. Vacuum layer of 12 A was used to separate the metal slabs. Then, the adsorption energy of the molecules was calculated by the following equation;

$$\Delta E_{ads} = E_{adsorbed\ system} - (E_{clean\ metal\ slab} + E_{gas})$$

Ultra-soft psuedopotentials[12] were employed within a cut off energy of 500 eV. Exchange correlation potential used in this calculation was Perdew Wang (PW-91),[13] and the electron density was converged within a tolerance of 1×10-5 eV. The Monkhorst-Pack scheme was used to generate k-point grid in the Brillouin zone, and the 7×7×1 k-point grid was adapted for both Pd(111) and Pd(100) slabs

Part II. Design and synthesis of novel blue phosphorescent host materials for organic light-emitting diode application

1. Introduction

Organic light-emitting diode (OLED) is considered next generation technology for lighting and panel displays because of their full-color emission, low driving voltages, rapid responses, low power consumptions and high contrasts.[1] OLED has self-luminescent capability, not needing extra backlight. This allows for the devices incorporating the OLED's as thin as 1 mm, much thinner than that of the Liquid Crystal Display (LCD), which has been the main display technology of choice so far. Furthermore, OLED's have simple manufacturing process and could be implemented as portable and/or flexible display.[2]

OLED devices have organic thin films containing organic light emitting layer between two electrodes. When 5 to 10 DC voltage is applied across the electrodes, the electron is injected from the cathode and holes are injected from the anode, which leads to the generation of excitons in organic layer. Then, the transition of exciton from excited states to ground states causes emission of visible light.[3] In excited states, the singlet excitons and the triplet excitons are observed, and the former emits fluorescent and the latter phosphorescent. Usually, the ratio of singlet and triplet is known to be 1:3. So the quantum efficiency of fluorescent OLED, which uses only the singlet excitons for light emission, is limited to 25%. On the other hand, phosphorescent OLED could utilize both the singlet and the triplet excitons for light emission, therefore theoretical quantum efficiency is expected to be higher than that of the fluorescent OLED by four times.

For efficient phosphorescent OLED, various high triplet energy charge transport host and high efficiency dopant materials have been developed.[4] Active research on phosphorescence materials has been carried out and 20% theoretical external quantum efficiency has already been achieved in red and

green phosphorescence. But there still is room for improvement in blue phosphorescence and further research on high triplet energy charge transport materials is required. For commercialization, stable and efficient blue phosphorescence materials have to be newly designed and synthesized.

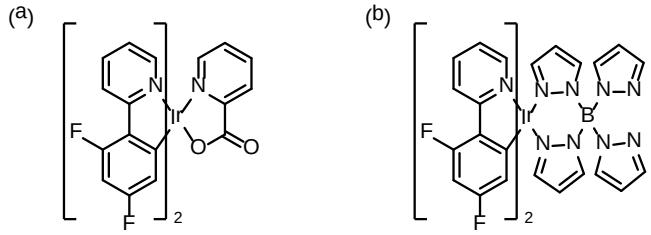

Figure 5. Common blue phosphorescent dopant materials: (a) Firpic and (b) Fir6

Presently available phosphorescent host materials are not suitable for deep blue phosphorescence due to their triplet energy level. Miss-matched combination of dopant and host materials results in incomplete energy transfer from the host to the deep blue emitting dopant materials and reverse energy transfer from dopant to host materials. The triplet energy of deep blue dopant is usually from 2.75 eV (Firpic, Fig. 1a) to 2.80 eV (FIr6, Fig. 1b) and the triplet energy of host should be higher than 2.85 eV and better be 2.95 eV for deep blue phosphorescence. And the OLED materials should satisfy the requirement for good film morphology with good evaporation property. A carbazole structure has been chosen to be a typical core structure for high triplet energy hole transport material because of good hole transport properties and high triplet energy (3.0 eV). The most widely used hole transport material containing carbazole core was *N,N′*-dicarbazoyl-3,5-benzene (mCP) which

has a high triplet energy of 2.9 eV. Various host materials that have been generally used are shown in Figure 2,[5] most of which do not have enough thermal, morphological stability and the quantum efficiency. Therefore, there is a need to develop novel host materials to satisfy the required options.

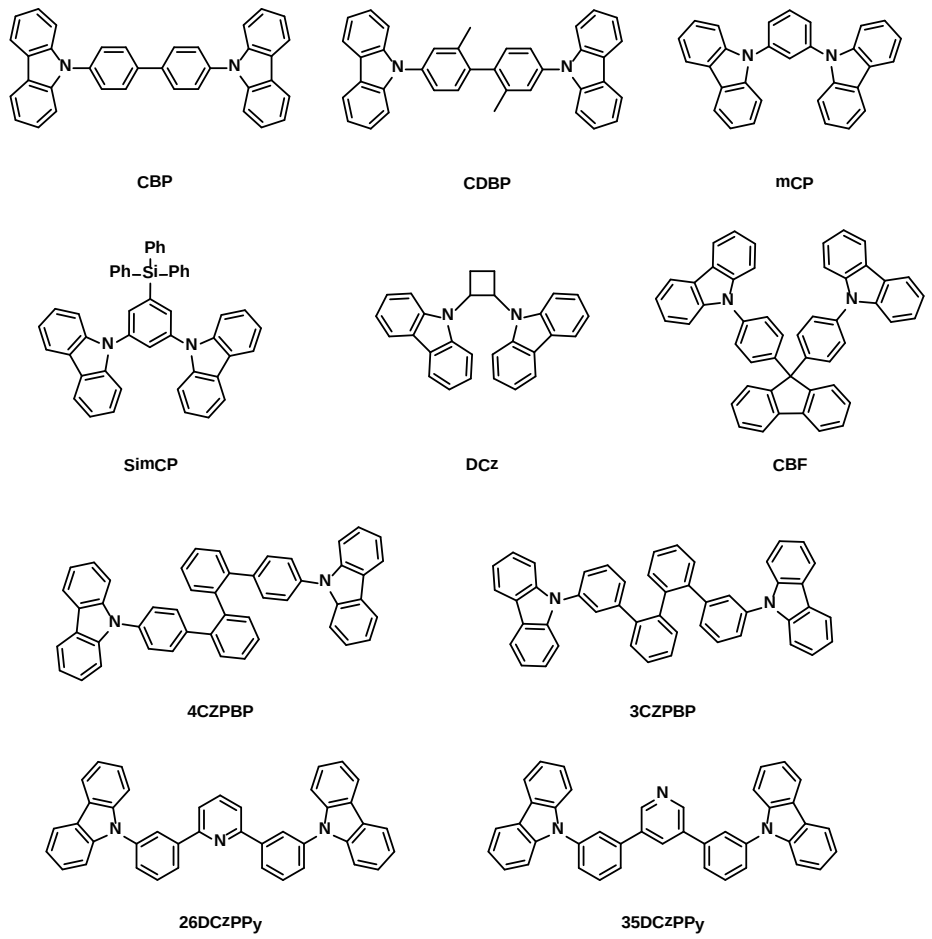

Figure 6. Commonly used host materials for OLED.

In this study, we designed novel structures for blue phosphorescent host materials, which exhibit high triplet energy level, high electron/hole transportation property and high mobility. The main goal is the development of new types of bipolar host materials, equipped with both electron donor and

acceptor in a single molecule (Fig. 3).[6] Device development tactics will be based on p- & n- type mixed host system as a baseline approach to achieve this daunting task for phosphorescent blue materials.

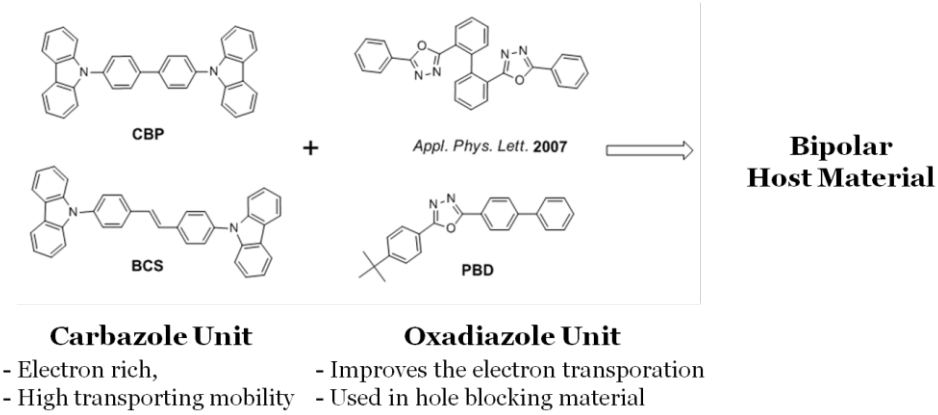

Figure 7. The concept of bipolar host materials

2. Results and Discussion

We designed new bipolar host material containing the electron donor and acceptor moieties to endow high triplet energy level and high electron/hole transportation mobility. As an electron donor, we chose the carbazole unit which has electron rich property and high transporting mobility. So we prepared various carbazole derivatives prior to the synthesis of target molecule (Scheme 1).

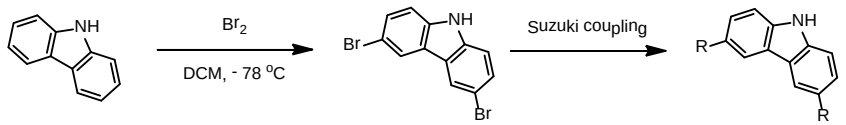

1

2a: R = 1-naphthyl
2b: R = 4-*t*-butylphenyl

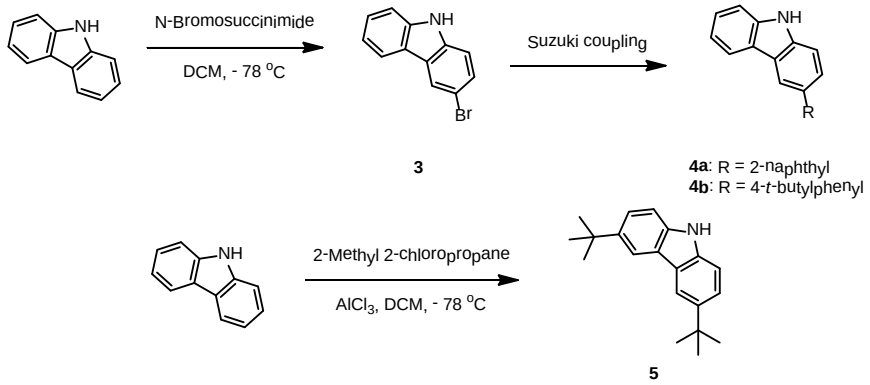

Scheme 1. Preparation of various carbazole derivatives

In case of an electron acceptor, we introduced oxadiazole or triazole unit to improve the electron transportation that are used in hole blocking materials. And since a red-shift was expected from full conjugation of aromatic ring in these compounds, we added methylene spacer between the electron donor and the acceptor group to break the conjugation. According to this concept, we designed and synthesized 11 compounds possessing the oxadiazole unit (Scheme 2, Fig. 4) and 3 compounds with the triazole unit (Scheme 3, Fig. 5)

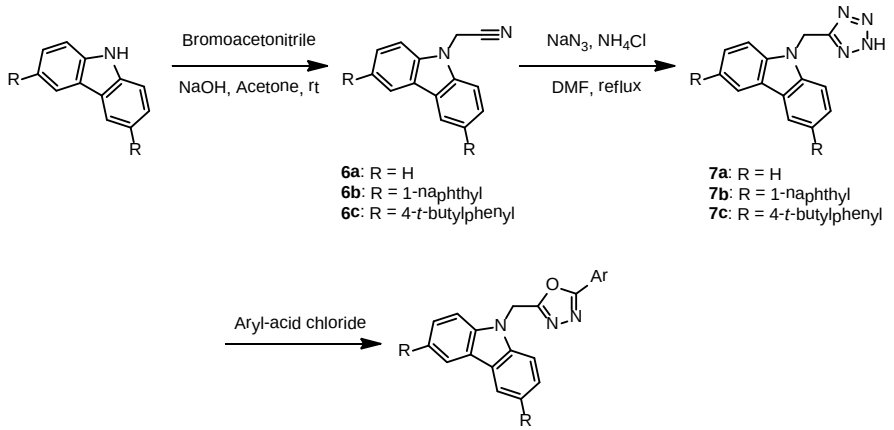

Scheme 2. A synthetic route of oxadiazole-containing compounds

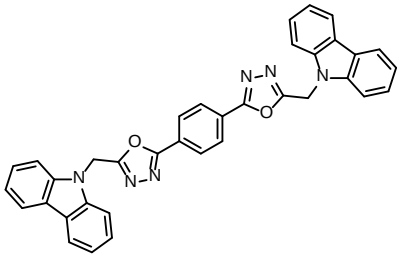

8

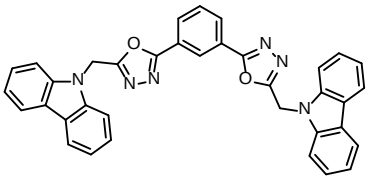

9

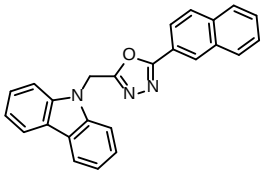

10

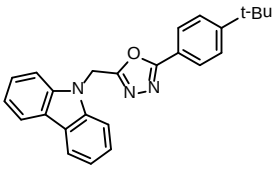

11

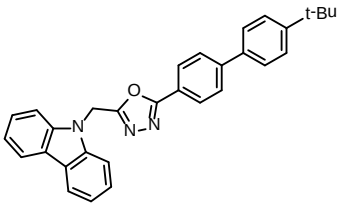

12

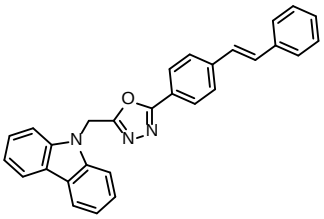

13

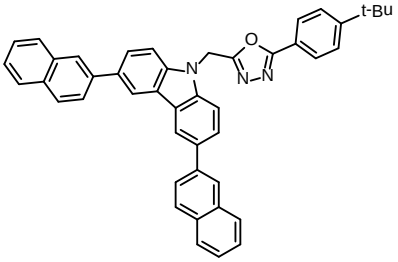

14

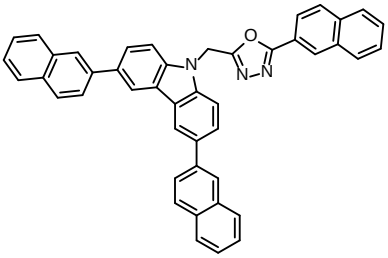

15

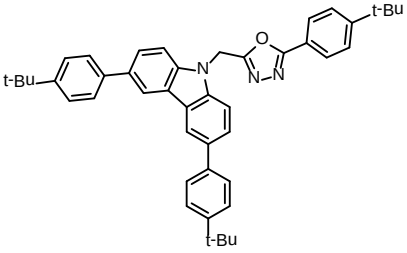

16

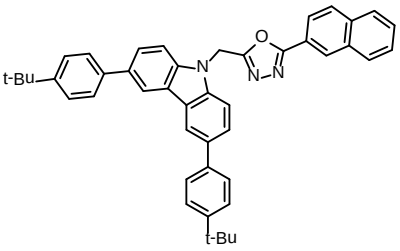

17

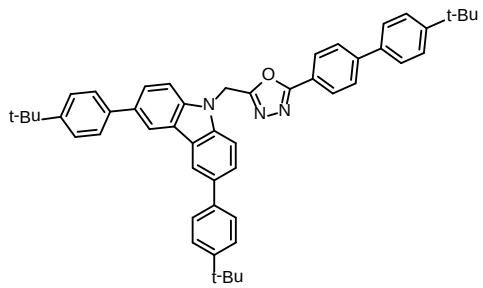

18

Figure 8. Synthesized compounds containing oxadiazole unit.

Compound **7** incorporating a tetrazole group was synthesized from carbazole through two steps. This tetrazole group was replaced with oxadiazole derivatives by “Click” chemistry with various acid chlorides. The reaction with terephthalolyl chloride or isophthalolyl chloride generated compounds of dimer type (**8** and **9**). We added 1-naphthyl or 4-*t*-butylphenyl group on the 3,6-position of carbazole to increase solubility and molecular weight (compounds **14-18**). The triazole-containing compounds were synthesized through Click chemistry as shown in Figure 5.

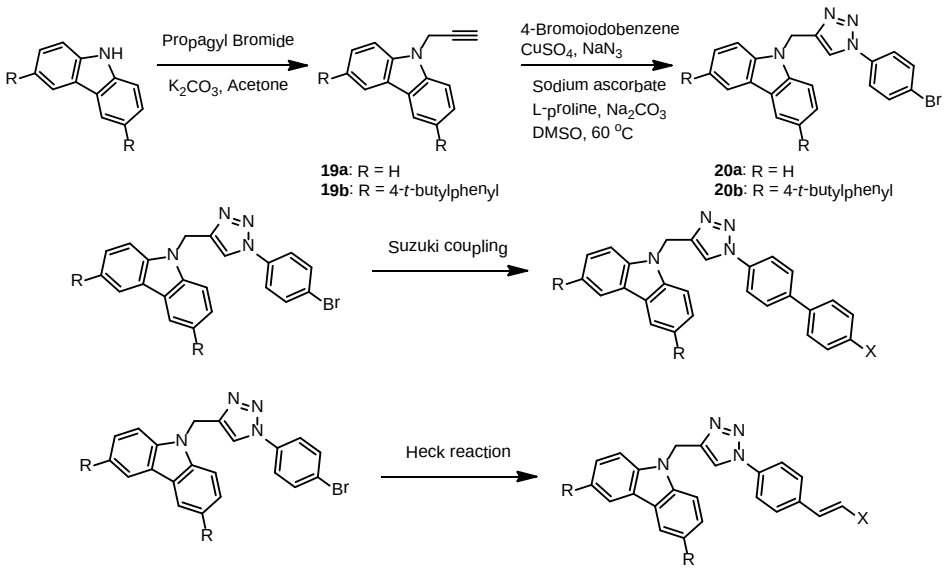

Scheme 3. A synthetic route to triazole-containing compounds

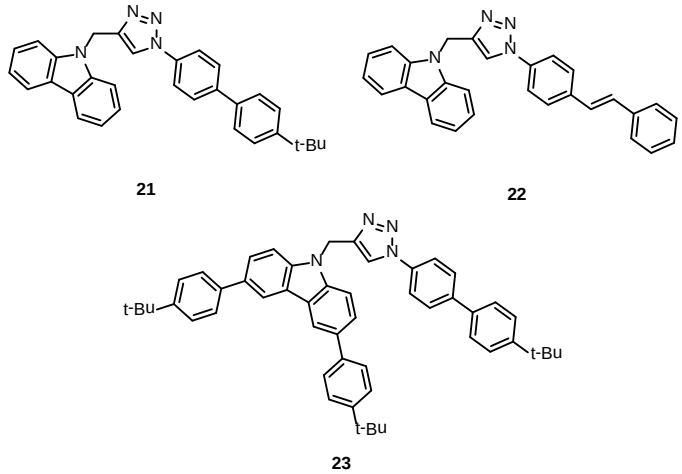

Figure 9. Synthesized compounds containing triazole unit.

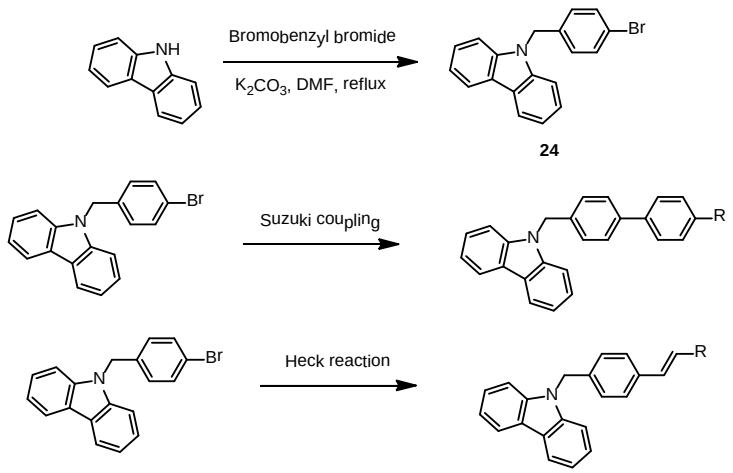

Scheme 4. A synthetic route of compounds including benzyl linker.

We designed compounds incorporating a benzyl linker and compound **24** was prepared as an intermediate. Suzuki coupling and Heck reaction on compound **24** were successful, but the low solubility of the products hindered us from having pure products. Therefore the synthetic route in the Scheme 4 was abandoned.

Among 14 compounds synthesized, four compounds were selected for testing. As shown in Table 1 and 2, overall, the results fell short of our expectations. The purities of samples (99.0%) were shy of the desired 99.9% purity of the reference sample. In addition, the difference between the highest occupied molecular orbital (HOMO) and the lowest unoccupied molecular orbital (LUMO) was too high when compared with the reference (PBH 235)

Table 1. Characterization results of samples (Oxadiazole and triazole unit)

Sample name	**Purity(%)**	**HOMO**	**LUMO**	**T_g**	**T_m**
PBH235(Ref)	99.9	5.94	2.64	150	N. D.
Compound **8**	99.0	5.85	2.41	122	330
Compound **16**	99.1	5.43	1.78	N. D.	250
Compound **17**	99.3	5.53	1.99	137	N. D.
Compound **21**	99.0	5.59	1.83	130	262

Table 2. Device performance of samples (Oxadiazole and triazole unit)

Sample name	**Luminance(Cd/m^2)**	**Voltage**	**Cd/A**	**Lm/W**	**CIE(x/y)**
PHB235(Ref)	450	4.88	4.62	2.90	(0.152/0.223)
Compound **8**	49	4.46	0.49	0.34	(0.171/0.200)
Compound **16**	31	4.16	0.31	0.24	(0.185/0.272)
Compound **17**	21	4.52	0.21	0.15	(0.210/0.185)
Compound **21**	9	4.21	0.09	0.07	(0.181/0.258)

None of the compounds showed desirable device performance as compared with the desired specification. There is no significant light-emitting from the devices incorporating our samples presumably due to low purity, which leads to the decomposition of compounds. The problems were considered to be caused by structural instability of the triazole unit and the air-oxidation of the

methylene spacer. Further, perhaps more meticulous purification methods were required and the molecular structure should be modified to warrant improved stability. We then decided to reevaluate the bipolar structure considering the moderate result from the color coordinate and driving voltage.

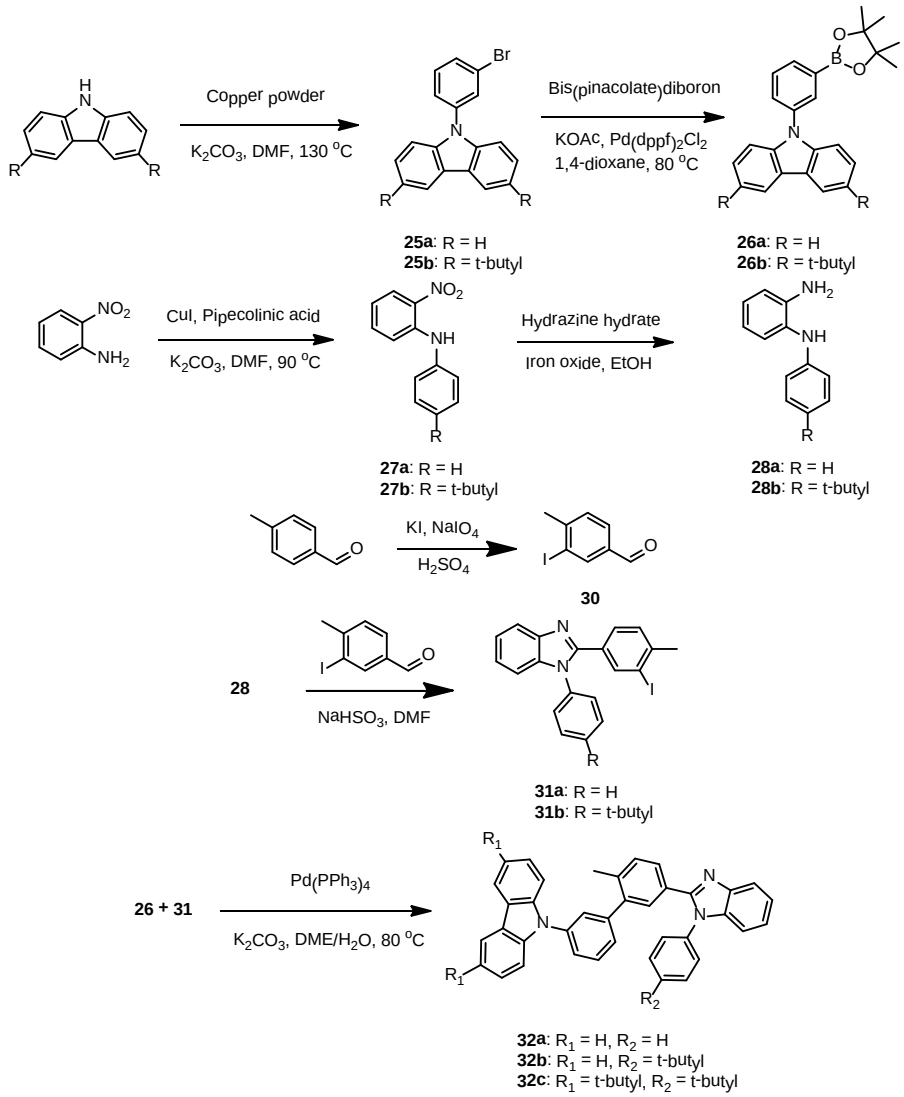

Scheme 5. A synthetic route of host materials incorporating a benzimidazole moiety

Based on the previous work, bipolar type compound containing carbazole/heterocycle units with methylene spacer were considered to have problems that are related to instability by oxidation of methylene and local charge transfer. However the bipolar structure was considered to be a valid design element and we devised new bipolar type compounds with no methylene spacer. Since removal of the methylene spacer could cause a red shift, instead, we added substituted phenyl groups and changed substitution patterns to break off the full conjugation of the aromatic rings. Benzimidazole group was selected as a new heterocycle unit and substitution positions were changed from para to meta as shown in Scheme 5.

Table 3. Device performance of PH-220 (Compound **32b**)

Dopant : Firpic					
@10 mA/cm^2	**CIE x**	**CIE y**	**V**	**Cd/A**	**Lm/W**
PH-220	0.144	0.323	6.64	11.44	5.41
mCP	0.146	0.322	6.20	12.12	6.14
Dopant : FIr6					
@10 mA/cm^2	**CIE x**	**CIE y**	**V**	**Cd/A**	**Lm/W**
PH-220	0.152	0.256	6.58	3.05	1.46
mCP	0.147	0.247	6.52	7.47	3.60
Device structure: Anode/LG HTL1/LG HTL2/HTL/EBL/Host+Dopant 8%/HBL/LG ETL/cathode					

After characterization, Compound **32b** was selected as a new host material for device testing. A display device using PH-220 (Compound **32b**) showed a

comparable result in its performance with FIrpic dopant, although the performance with FIr6 Dopant was disappointing (Table 3).

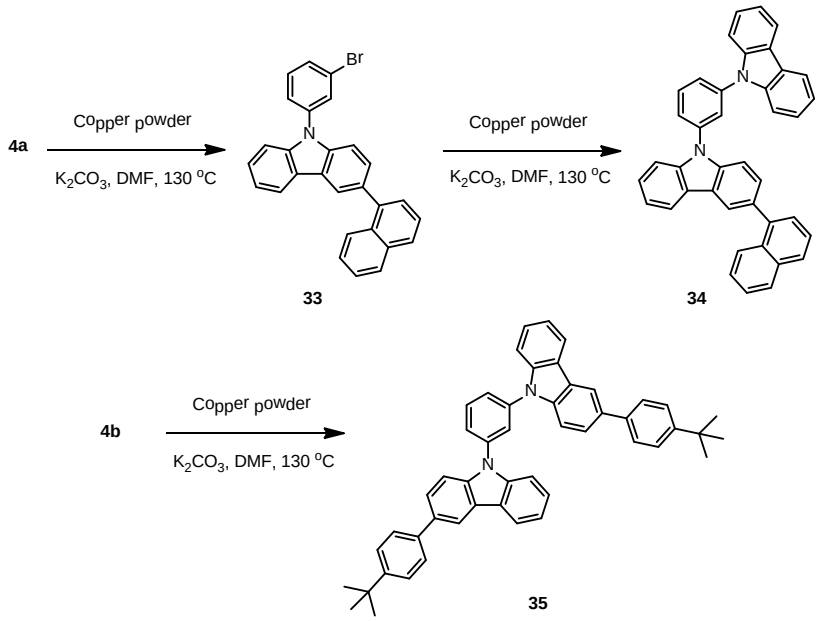

Scheme 6. A synthetic route of mCP derivatives.

Considering the triplet energy level, the benzimidazole unit was considered not appropriate for blue phosphorescent host. Focusing on the color coordinate and efficiency, we came up with new compounds, **34** and **35**. Compounds **34** and **35**, which are derivatives of mCP (*N*,*N'*-dicarbazolyl-3,5-benzene), have a substitution on the 3-position of carbazole and high triplet energy level. Figure 6 shows the UV–vis absorption, solution PL spectra of compound 34. UV–vis absorption peaks were observed at 245 nm and 295 nm. The solution PL spectrum was measured in dichloromethane, and the maximum emission peak was observed at 382 nm. Since compound **34** showed the highest purity and good optical property, we tested onto devise and the result is shown in Table 4. This device has suitable color coordinate values for deep blue emission (0.15, 0.17). The efficiencies and maximum

luminance for this device are comparable with those of the existing OLED materials.

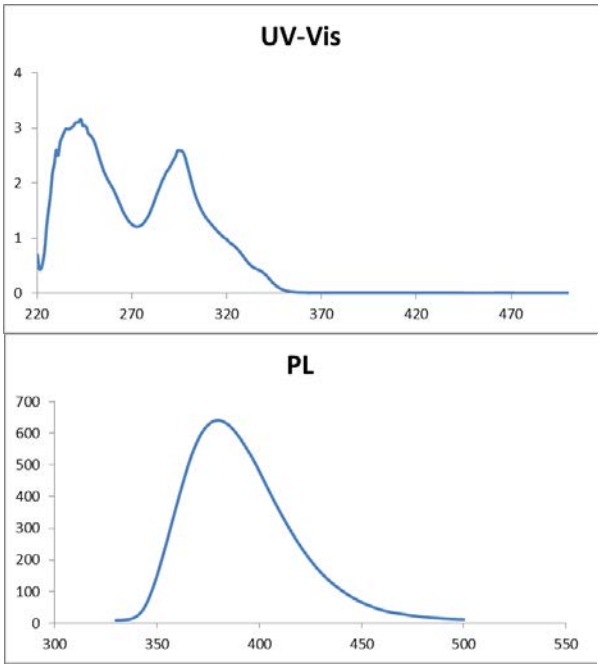

Figure 10. UV–vis absorption, PL spectra of compound **34**

Table 4. Device performance of BMK-552(compound **34)**

Materials	V_{op}	Cd/A	Lm/W	EQE(%)	CIE x	CIE y
Dopant (8%)	3.5	7.4	6.7	6.0	0.148	0.173
Dopant (10%)	3.5	8.3	7.4	6.6	0.154	0.174
Dopant (12%)	4.0	9.6	7.4	7.3	0.149	0.190
Dopant (14%)	4.0	9.0	7.0	6.8	0.148	0.194

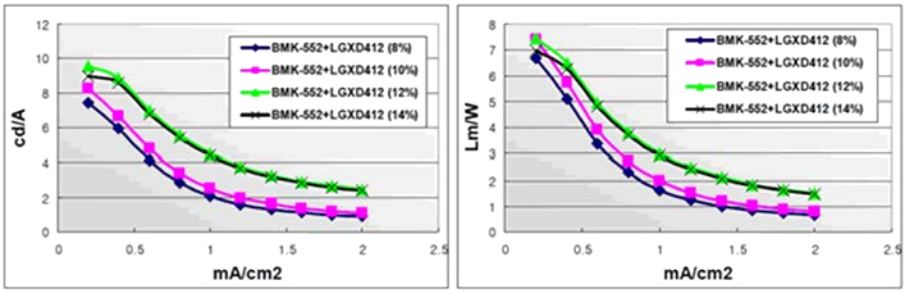

3. Conclusion

A series of noble blue phosphorescence materials were successfully prepared for OLED host material. Totally 29 compounds were designed and synthesized and 24 compounds were evaluated as host materials for blue OLED. Some of the newly prepared compounds showed superior luminous efficiency and power efficiency, as well as blue color in CIE coordinates, compared to existing OLED materials. However, our products fell short of our final goal set for the single host requirement. Compound **32b** and **34** could be utilized as useful host materials in a mixed host system and further research is required.

4. Experimental

General Experiments

All reactions were performed under argon and stirring was carried out with magnetic stirring. Column chromatography was carried out using flash silica gel from Merck (230-400 mesh). Carbazole was purified by recrystallization.

OLED's were fabricated by vacuum deposition onto patterned ITO glass that had been thoroughly cleaned and subsequently treated with oxygen plasma. Blue phosphorescent OLED's were sequentially fabricated onto the ITO substrates through thermal evaporation of organic layers (evaporation rate: 2 Å/s; base pressure: 3×10^{-6} Torr). The EL spectra and CIE color coordinates were obtained using a Spectrascan PR650 photometer, and the current–voltage–luminescence (J–V–L) characteristics were measured using a Keithley 2400 source unit.

A synthesis procedure of compound 1

Carbazole (90 mmol) was dissolved in anhydrous CH_2Cl_2 (250 mL) and

added of N-bromosuccinimide (NBS, 270 mmol) at room temperature under argon atmosphere. The mixture was stirred at room temperature for 6 hours. After the reaction was done, the reaction mixture was quenched by addition of water. The crude was extraction with CH_2Cl_2 and washed with water. The combined organic layer was dried over anhydrous $MgSO_4$, filtered and concentrated under reduced pressure. Column chromatography on silica gel (hexane/ethyl acetate) afforded products as white solids (26.3 g, 89%). 1H NMR ($CDCl_3$): δ 7.38 (d, 2H), 7.57(dd, 2H), 8.12 (d, 2H), 8.31 (s, 1H, NH)

General procedure for Suzuki coupling

Degassed solvent (1,2-dimethoxyethane:H_2O=3:1), aryl halide (1.0 equiv), aryl boronic acid (1.2 equiv), base (1.3 equiv), and $Pd(PPh_3)_4$ (5 mol%) were added to a round-bottom flask, which was backfilled with argon. The reaction mixture was refluxed for 24 h with vigorous stirring. After the reaction, the reaction mixture was cooled to room temperature and the catalyst was separated using a magnet. The mixture containing products was extracted with methylene chloride and water. The organic layer was concentrated and purified through flash chromatography using hexane and ethyl acetate as an eluent.

General procedure for Heck reaction

Aryl halide (1.0 equiv), olefin (1.2 equiv), base (1.3 equiv), and $Pd(PPh_3)_4$ (5 mol%) were added to a round-bottom flask. The reaction mixture was stirred under argon atmosphere for 24 h at 110 ^oC. After the reaction, the mixture was cooled to room temperature and the catalyst was separated using a magnet. The mixture containing products was partitioned between methylene chloride and water and organic layer was concentrated. Column chromatography on silica gel (hexane/ethyl acetate) afforded products.

A synthesis procedure of compound 3

Carbazole (90 mmol) was dissolved in anhydrous CH_2Cl_2 (250 mL) and added of N-bromosuccinimide (NBS, 90 mmol) at -78 ^oC. The mixture was stirred at room temperature for 6 hours. After the reaction was done, the reaction mixture was quenched by addition of water. The crude was extraction with CH_2Cl_2 and washed with water. The combined organic layer was dried over anhydrous $MgSO_4$, filtered and concentrated under reduced pressure. Column chromatography on silica gel (hexane/ethyl acetate) afforded products as white solids (15.5, 71%). 1H NMR ($CDCl_3$): δ 7.29 (dd, 1H), 7.38 (d, 2H), 7.57(dd, 2H), 8.12 (d, 2H), 8.31 (s, 1H, NH)

A synthesis procedure of compound 5

9-H-carbazole (20 mmol), 100 ml of nitromethane, and $ZnCl_2$ (60 mmol) were added to a two-neck flask under a nitrogen atmosphere. 2-Chloro-2-methylpropane (60 mmol) was added dropwise under stirring. The mixture was stirred at room temperature for 5 hours and then hydrolyzed with 100 ml of water. The product was extracted with dichloromethane. The organic layer was washed with H_2O, dried with magnesium sulfate, and evaporated under vacuum. Column chromatography on silica gel (hexane/ethyl acetate) afforded products as white solids (4.3 g, 77%). 1H NMR ($CDCl_3$): δ 8.07 (d, J = 1.94 Hz, 2H), 7.83 (s b, 1H), 7.49(dd, J= 8.46, 1.93 Hz, 2H), 7.33 (dd, J = 5.56, 0.49 Hz, 2H), 1.44 (s, 18H).

A synthesis procedure of compound 6

To a flame-dried 250mL round-bottle flask, carbazole (100 mmol) was added then dissolved in acetone. Then bromoacetonitrile (120 mmol), NaOH (200 mmol) were added to the solution. The mixture was stirred at room

temperature. After 12 hours, reaction mixture was quenched with water and extracted twice with ether. The combined organic extracts were dried ($MgSO_4$) and concentrated by rotary evaporation. Column chromatography on silica gel (hexane/ethyl acetate) afforded products as white solids (12.4 g, 60%).

A synthesis procedure of compound 7

Under reflux, a suspension of solid of Compound **6** (1.0 equiv) in dimethylformamide was added into a flask containing with sodium azide (1.5 equiv) and Ammonium chloride (1.5 equiv). The mixture was refluxed for 24 hours, and then quenched with water after cooling back to room temperature and extracted twice with ether. The combined organic extracts were dried ($MgSO_4$) and concentrated by rotary evaporation. Column chromatography on silica gel (hexane/ethyl acetate) afforded products as white solids.

A synthesis procedure of compound 8

To an oven-dried, 500ml two-neck round bottom flask, magnetic stir bar was equipped. Then compound **4a** (15 g, 60 mmol), terephthaloyl chloride (6.1 g, 30 mmol) and triethyl amine (20 mL, 180 mmol) were added then dissolved in pyridine (200 mL). The mixture was refluxed for 6 hours, and then quenched with water after cooling back to room temperature and extracted twice with dichloromethane. The combined organic extracts were dried by magnesium sulfate and concentrated by rotary evaporation. Column chromatography on silica gel (dichloromethane: methanol=9:1) afforded products as white solids (13.0 g, 76 %). 1H NMR ($CDCl_3$): δ 8.13-8.07 (m, 4H), 7.85 (s, 4H), 7.70 (d, J =8.2 Hz, 4H), 7.53-7.42 (m, 4H), 7.31-7.25 (m, 4H), 5.71 (s, 4H).

General procedure for synthesis of compound 8-18 (Click chemistry)

To an oven-dried, 500ml two-neck round bottom flask, magnetic stir bar was equipped. Then compound **4** (1.0 equiv), acid chloride (1.0 equiv) and triethyl amine (3.0 equiv) were added then dissolved in pyridine. The mixture was refluxed for 6 hours, and then quenched with water after cooling back to room temperature and extracted twice with dichloromethane. The combined organic extracts were dried by magnesium sulfate and concentrated by rotary evaporation. Column chromatography on silica gel (hexane/ethyl acetate) afforded products as solids.

A synthesis procedure of compound 19

To a flame-dried 250 mL round-bottle flask, carbazole (87 mmol) was added then dissolved in acetone. Then propagyl bromide (100 mmol), K_2CO_3 (150 mmol) were added to the solution. The mixture was stirred at room temperature. After 12 hours, reaction mixture was quenched with water and extracted twice with ether. The combined organic extracts were dried ($MgSO_4$) and concentrated by rotary evaporation. Column chromatography on silica gel (hexane/ethyl acetate) afforded products as white solids (9.5 g, 53%).

A synthesis procedure of compound 20

4-bromoiodobenzene (103 mg, 0.5 mmol, 1 equiv) is mixed with compound **19** (56 mg, 0.5 mmol, 1 equiv) in a 100 mL round-bottle flask. To the mixture were added *L*-proline (12 mg, 0.1 mmol, 0.2 equiv), Na_2CO_3 (12 mg, 0.1 mmol, 0.2 equiv), NaN_3 (39 mg, 0.6 mmol, 1.2 equiv), sodium ascorbate (20 mg, 0.05 mmol, 0.1 equiv), DMSO (1 mL), and $CuSO_4$ (13 mg, 0.025 mmol, 0.05 equiv). The mixture was heated overnight at 65 ^oC for 3 hours. The crude mixture was poured into water and extracted with ethyl acetate. The organic layer was washed with brine and dried over $MgSO_4$. Column chromatography on silica gel (hexane/ethyl acetate) afforded products as white solids.

A synthesis procedure of compound 24

To a flame-dried 250 mL round-bottle flask, carbazole (6.8 mmol) was added then dissolved in acetone. Then bromobenzyl bromide (5.6 mmol), K_2CO_3 (28 mmol) were added to the solution. The mixture was refluxed for 12 hours and then quenched with water and extracted twice with ether. The combined organic extracts were dried ($MgSO_4$) and concentrated by rotary evaporation. Column chromatography on silica gel (hexane/ethyl acetate) afforded products as white solids (1.8 g, 78%).

A synthesis procedure of compound 25

A mixture of 1-bromo-3-iodobenzene (35 mmol), carbazole (52 mmol), copper powder (159 mmol) and potassium carbonate (159 mmol) in DMF was stirred at 130 °C for 24 hours under Argon atmosphere. After cooling to room temperature, the reaction mixture was diluted with ethyl acetate and filtered through celite. The filtrate was poured into water and then extracted with ethyl acetate. The combined organic extracts were dried ($MgSO_4$) and concentrated by rotary evaporation. Column chromatography on silica gel (hexane/ethyl acetate) afforded products as white solids. 1H NMR ($CDCl_3$): δ 8.13 (d, 2H), 7.75 (s, 1 H), 7.61 (d, 1 H), 7.53 (d, 1 H), 7.49 (d, 1H), 7.42 (m, 4H), 7.27-7.31 (m, 2H)

A synthesis procedure of compound 26

A mixture of compound **25** (9.3 mmol), bis(pinacolato)diboron (26 mmol), potassium acetate (98 mmol) and 1,1'-Bis (diphenylphosphino)ferrocene-palladium(II)dichloride (1.5 mmol) complex with dichloroethane in dioxane was stirred at 80 °C for 24 hours under argon atmosphere. After cooling to room temperature, the reaction mixture was filtered through celite. The filtrate

was poured into water and then extracted with ethyl acetate. Column chromatography on silica gel (hexane/ethyl acetate) afforded products as white solids. 1H NMR ($CDCl_3$): δ 1.35 (s, 12H), 7.25-7.29 (m, 2H), 7.32 (d, 2H),7.44-7.45 (d, 2H), 7.5-7.64 (m, 2H), 7.86-7.87 (d, 1H), 7,99 (s, 1H), 8.13 (s,2H)

A synthesis procedure of compound 27

To an oven-dried, 500 mL two-neck round bottom flask, magnetic stir bar was equipped. Then CuI (8.7 mmol) and pipecolinic acid (17.4 mmol) were added then dissolved in DMF (0.5 M). The solution was degassed with Ar bubbling for 10 min the under Ar atmosphere, 2-nitroaniline (72.4 mmol), bromo-4-tertbutylbenzene (43.4 mmol) and potassium carbonate (144.8 mmol) were added. The resulted mixture was heated to 110 °C. After cooling to room temperature, the reaction mixture was filtered through celite. The filtrate was poured into water and then extracted with ethyl acetate. Column chromatography on silica gel (hexane/ethyl acetate) afforded products as yellow solids (10.9 g, 93%). 1H NMR ($CDCl_3$): δ 1.35 (s, 9H), 6.69-6.77 (m, 1H), 7.16-7.23 (m, 3H), 7.30-7.38 (m, 1H), 7.43 (d, J = 8.6 Hz,2H), 8.18 (dd, J = 8.6, 1.5 Hz, 1H), 9.46 (s, 1H)

A synthesis procedure of compound 28

To an ethanol solution of compound **27** (1.8 mmol), Pd/C (10 wt%) and Hydrazine monohydrate (1 ml/g) were added. Then heated to 80 °C. After the completion of the reaction, the reaction mixture was filtered then filtrate was diluted with water to precipitate the product (0.43 g, 98%) 1H NMR ($CDCl_3$): δ 1.29 (s, 9H), 3.75 (s, 2H), 5.12(s, 1H), 6.71-6.76 (m, 3H), 6.79-6.81 (d, 1H), 6.98-7.01 (t, 1H), 7.11-7.12 (d, 1H), 7.23-7.25 (d, 2H)

A synthesis procedure of compound 30

Sodium periodate (55 mmol) and potassium iodide (165 mmol) were added slowly to stirred conc. H_2SO_4. Stirring was continued for 30 min at room temperature. p-Tolualdehyde (200 mmol) was suspended in stirred conc.H_2SO_4 at rt. The iodinating solution was added dropwise over 1 hour. Then this solution was stirred 1 hour and poured into 1L flask with 500g ice. 1H NMR ($CDCl_3$): δ 2.44 (s, 3H), 7.32-7.34 (d, 2H), 7.76-7.79 (d, 2H), 9.96 (s, 1H)

A synthesis procedure of compound 31

To an oven-dried 500ml round-bottle flask, compound 28 (28.5 mmol) was charged then dissolved in DMF (0.2 M). Then to the solution, compound **30** (50 mmol) and sodium bisulfite (104 mmol) were added. The reaction mixture was heated to 110 °C under Ar atmosphere for 24 hours. After cooling to room temperature, the reaction mixture was diluted with ethyl acetate and filtered through celite. The filtrate was poured into water and then extracted with ethyl acetate. The combined organic extracts were dried ($MgSO_4$) and concentrated by rotary evaporation. Column chromatography on silica gel (hexane/ethyl acetate) afforded products as white solids. 1H NMR ($CDCl_3$): δ 1.4 (s, 9H), 2.4 (s, 3H), 7.13-7.14 (s, 1H), 7.22-7.24 (m, 4H), 7.33 (s, 1H), 7.43-7.45 (d, 1H), 7.53-7,54 (d, 2H), 7.87-7.88 (d, 1H),7.99 (s, 1H)

A synthesis procedure of compound 32b

To an oven-dried 50ml two-neck round-bottle flask, DME and water were added then degassed with argon gas for 10 min. Then under argon atmosphere, compound **31b** (2.2 mmol), compound **26a** (2.2 mmol) and potassium carbonate (4.3 mmol) were added. This reaction mixture was heated to 80 °C. Finally $Pd(PPh_3)_4$ (0.22mmol) was added to the mixture and stirred for 24

hours. After cooling to room temperature, the reaction mixture was diluted with dichloromethane and filtered through celite. The filtrate was poured into water and then extracted with dichloromethane. The combined organic extracts were dried ($MgSO_4$) and concentrated by rotary evaporation. Column chromatography on silica gel (hexane/ethyl acetate) afforded products as white solids (0.92 g, 73%). 1H NMR ($CDCl_3$): δ 1.25 (s, 9H), 2.38 (s,3H), 7.13-7.14 (d, 1H), 7.25-7.33 (m, 4H), 7.34-7.37 (m, 4H), 7.39-7.45 (m,8H), 7.49-7.51 (d, 1H), 7.54-7.57 (t, 1H), 7.59-7.61 (d,1H), 7.87-7.89 (d, 1H),8.14-8.15 (d, 2H)

A synthesis procedure of compound 32c

To an oven-dried two-neck round-bottle flask, DME and H_2O were added and degassed with argon gas for 10 min. Then under argon atmosphere, compound **31b** (11.2 mmol), compound **26b** (11.2 mmol) and Na_2CO_3 (22.5 mmol) were added. The reaction mixture was heated to 80 °C. Finally $Pd(PPh_3)_4$ (10 mol%) was added to the mixture and stirred for 24 hours. After cooling to room temperature, the reaction mixture was diluted with dichloromethane and filtered through celite. The filtrate was poured into water and then extracted with dichloromethane. The combined organic extracts were dried ($MgSO_4$) and concentrated by rotary evaporation. Column chromatography on silica gel (hexane/ethyl acetate) afforded products as white solids (5.34 g, 69%). 1H NMR ($CDCl_3$): δ 1.26 (s, 9H), 1.44-1.46 (s, 18H), 2.36 (s, 3H), 7.07 (d, 1H), 7.25-7.26 (s, 5H), 7.33-7.35 (m, 4H), 7.37 (s, 1H), 7.42-7.52 (m, 6H), 7.59 (d, 1H),7.87 (d, 1H), 8.13 (s, 2H)

A synthesis procedure of compound 33

A mixture of 1-bromo-3-iodobenzene (35 mmol), compound **4a** (52 mmol), copper powder (159 mmol) and potassium carbonate (159 mmol) in DMF was

stirred at 130 °C for 24 hours under nitrogen atmosphere. After cooling to room temperature, the reaction mixture was diluted with ethyl acetate and filtered through celite. The filtrate was poured into water and then extracted with ethyl acetate. The combined organic extracts were dried ($MgSO_4$) and concentrated by rotary evaporation. Column chromatography on silica gel (hexane/ethyl acetate) afforded products as white solids.

A synthesis procedure of compound 34

To an oven-dried two-neck round-bottle flask, compound **33**, carbazole, copper powder and potassium carbonate are dissolved in 1,2-dichloro-benzene under nitrogen atmosphere. The reaction mixture was heated to 100°C for 12 hours. After cooling to room temperature, the reaction mixture was diluted with dichloromethane and filtered through celite. The filtrate was poured into water and then extracted with dichloromethane. The combined organic extracts were dried ($MgSO_4$) and concentrated by rotary evaporation. Column chromatography on silica gel (hexane/ethyl acetate) afforded products as white solids. 1H NMR ($CDCl_3$): δ 7.25-7.33 (m, 5H), 7.44-7.55 (m, 7H), 7.61-7.69 (m, 3H), 7.77 (s, 1H), 7.87-7.94 (m, 3H), 8.04-8.12 (m, 3H), 8.42(m, 1H), 8.55 (m, 3H)

A synthesis procedure of compound 35

To an oven-dried two-neck round-bottle flask, compound **4b**, 1,3-dibromobenzene, copper, potassium carbonate are dissolved in 1,2-dichloro-benzene. The reaction mixture was heated to 100°C for 12 hours under nitrogen atmosphere. After cooling to room temperature, the reaction mixture was diluted with dichloromethane and filtered through celite. The filtrate was poured into water and then extracted with dichloromethane. The combined organic extracts were dried ($MgSO_4$) and concentrated by rotary evaporation.

Column chromatography on silica gel (hexane/ethyl acetate) afforded products as white solids. 1H NMR ($CDCl_3$): δ 1.35 (s, 18H), 7.25-7.33 (m, 4H), 7.37-7.50 (m, 12H), 7.69 (d, 2H), 7.77(s, 2H), 7.87 (m, 2H), 7.94 (m, 2H), 8.55 (d, 2H)

Reference

Part I. Chapter 1

1. a) Heck, R. F.; Nolley, J. P. *J. Org. Chem.* **1972**, *37*, 2320; b) Dieck, H. A.; Heck, F. R. *J. Organomet. Chem*. **1975**, *93*, 259; c) Sonogashira, K.; Tohda, Y.; Hagihara, N. *Tetrahedron Lett.* **1975**, *16*, 4467; d) Baba, S.; Negishi, E. *J. Am. Chem. Soc*. **1976**, *98*, 6729; e) Milstein, D.; Stille, J. K. *J. Am. Chem. Soc.* **1978**, *100*, 3636; f) Miyaura, N.; Yamada, K.; Suzuki, A. *Tetrahedron Lett.* **1979**, *20*, 3437; g) Guram, A. S.; Buchwald, S. L. *J. Am. Chem. Soc.* **1994**, *116*, 7901; h) Paul, F.; Patt, J.; Hartwig, J. F. *J. Am. Chem. Soc*. **1994**, *116*, 5969.

2. a) Smidt, J.; Hafner, W.; Jira, R.; Sedlmeier, J.; Sieber, R.; Rüttinger, R.; Kojer, H. *Angew. Chem.* **1959**, *71*, 176; b) Stahl, S. S.; Thorman, J. L.; Nelson, R. C.; Kozee, M. A. *J. Am. Chem. Soc*. **2001**, *123*, 7188; c) Blaser, H.-U.; Malan, C.; Pugin, B.; Spindler, F.; Steiner, H.; Studer, M. *Adv. Synth. Catal*. **2003**, *345*, 103; d) Steinhoff, B. A.; Guzei, I. A.; Stahl, S. S. *J. Am. Chem. Soc.* **2004**, *126*, 11268; e) Stahl, S. S. *Science* **2005**, *309*, 1824; f) Gligorich, K. M.; Sigman, M. S. *Chem. Commun.* **2009**, 3854; g) Jira, R. *Angew. Chem. Int. Ed* **2009**, *48*, 9034; h) Campbell, A. N.; Stahl, S. S. *Acc Chem. Res.* **2012**, *45*, 851.

3. a) Kotha, S.; Lahiri, K.; Kashinath, D. *Tettrahedron* **2002**, *58*, 9633; b) Littke, A. F.; Fu, G. C. *Angew. Chem. Int. Ed* **2002**, *41*, 4176; c) Nicolaou, K. C.; Bulger, P. G.; Sarlah, D. *Angew. Chem. Int. Ed* **2005**, *44*, 4442; d) Chinchilla, R.; Najera, C. *Chem. Rev.* **2007**, *107*, 874; e) Lyons, T. W.; Sanford, M. S. *Chem. Rev.* **2010**, *110*, 1147; f) Köhler, K., Wussow, K. and Wirth, A. S. (2013) Palladium-Catalyzed Cross-Coupling Reactions – A

General Introduction, in Palladium-Catalyzed Coupling Reactions: Practical Aspects and Future Developments (ed Á. Molnár), Wiley-VCH Verlag GmbH & Co. KGaA, Weinheim, Germany.

4. Astruc, D. *Inorg. Chem.* **2007**, *46*, 1884.

5. a) Murzin, D. Y.; Mäki-Arvela, P.; Toukoniitty, E.; Salmi, T. *Catal. Rev.* **2005**, *47*, 175; b) Seki, M. *Synthesis* **2006**, *2006*, 2975; c) Yin, L.; Liebscher, J. *Chem. Rev.* **2007**, *107*, 133; d) Beletskaya, I.; Tyurin, V. *Molecules* **2010**, *15*, 4792; e) Lamblin, M.; Nassar-Hardy, L.; Hierso, J.-C.; Fouquet, E.; Felpin, F.-X. *Adv. Synth. Catal.* **2010**, *352*, 33; f) Mora, M.; Jiménez-Sanchidrián, C.; Rafael Ruiz, J. *Curr. Org. Chem.* **2012**, *16*, 1128.

6. a) Wong, H.-t.; Pink, C. J.; Ferreira, F. C.; Livingston, A. G. *Green Chem.* **2006**, *8*, 373; b) Hagiwara, H.; Ko, K. H.; Hoshi, T.; Suzuki, T. *Chem. Commun.* **2007**, 2838; c) Li, F.; Xia, C. *Tetrahedron Lett.* **2007**, *48*, 4845; d) Zhang, Y.; Quek, X.-Y.; Wu, L.; Guan, Y.; Hensen, E. J. *J. Mol. Catal. A: Chem.* **2013**, *379*, 53.

7. a) Abu-Reziq, R.; Avnir, D.; Miloslavski, I.; Schumann, H.; Blum, J. *J. Mol. Catal. A: Chem.* **2002**, *185*, 179; b) Lee, D.; Lee, H.; Kim, S.; Yeom, C.-E.; Kim, B. M. *Adv. Synth. Catal.* **2006**, *348*, 1021.

8. a) Fenger, I.; Le Drian, C. *Tetrahedron Lett.***1998**, *39*, 4287; b) Kohler, K.; Heidenreich, R. G.; Krauter, J. G.; Pietsch, J. *Chemistry* **2002**, *8*, 622; c) Lysén, M.; Köhler, K. *Synlett* **2005**, 1671; d) Stevens, P. D.; Fan, J.; Gardimalla, H. M.; Yen, M.; Gao, Y. *Org. Lett.* **2005**, *7*, 2085; e) Stevens, P. D.; Li, G.; Fan, J.; Yen, M.; Gao, Y. *Chem. Commun.* **2005**, 4435; f) Cassez, A.; Ponchel, A.; Hapiot, F.; Monflier, E. *Org. Lett.* **2006**, *8*, 4823; g) Webb, J.; Macquarrie, S.; McEleney, K.; Crudden, C. *J. Catal.* **2007**, *252*, 97; h) Yinghuai, Z.; Peng, S. C.; Emi, A.; Zhenshun, S.; Monalisa; Kemp, R. A. *Adv. Synth. Catal.* **2007**, *349*, 1917; i) Jana, S.; Dutta, B.; Bera, R.; Koner, S.

Inorg. Chem. **2008**, *47*, 5512; j) Liu, J.; Peng, X.; Sun, W.; Zhao, Y.; Xia, C. *Org. Lett.* **2008**, *10*, 3933; k) Laska, U.; Frost, C. G.; Price, G. J.; Plucinski, P. K. *J. Catal.* **2009**, *268*, 318; l) Scheuermann, G. M.; Rumi, L.; Steurer, P.; Bannwarth, W.; Mulhaupt, R. *J. Am. Chem. Soc.* **2009**, *131*, 8262; m) Wan, Y.; Wang, H.; Zhao, Q.; Klingstedt, M.; Terasaki, O.; Zhao, D. *J. Am. Chem. Soc.* **2009**, *131*, 4541; n) Siamaki, A. R.; Khder, A. E. R. S.; Abdelsayed, V.; El-Shall, M. S.; Gupton, B. F. *J. Catal.* **2011**, *279*, 1; o) Wang, Y.; Liu, J.; Xia, C. *Tetrahedron Lett.* **2011**, *52*, 1587; p) Akai, Y.; Yamamoto, T.; Nagata, Y.; Ohmura, T.; Suginome, M. *J. Am. Chem. Soc.* **2012**, *134*, 11092; q) Kılıç, B.; Şencanlı, S.; Metin, Ö. *J. Mol. Catal. A: Chem.* **2012**, *361-362*, 104; r) Zhu, W.; Yang, Y.; Hu, S.; Xiang, G.; Xu, B.; Zhuang, J.; Wang, X. *Inorg. Chem.* **2012**, *51*, 6020.

9. a) Astruc, D.; Lu, F.; Aranzaes, J. R. *Angew. Chem. Int. Ed* **2005**, *44*, 7852; b) Fihri, A.; Bouhrara, M.; Nekoueishahraki, B.; Basset, J. M.; Polshettiwar, V. *Chem. Soc. Rev.* **2011**, *40*, 5181.

10. Polshettiwar, V.; Luque, R.; Fihri, A.; Zhu, H.; Bouhrara, M.; Basset, J. M. *Chem. Rev.* **2011**, *111*, 3036.

11. a) Gu, H.; Zheng, R.; Zhang, X.; Xu, B. *J. Am. Chem. Soc.* **2004**, *126*, 5664; b) Figuerola, A.; Fiore, A.; Di Corato, R.; Falqui, A.; Giannini, C.; Micotti, E.; Lascialfari, A.; Corti, M.; Cingolani, R.; Pellegrino, T.; Cozzoli, P. D.; Manna, L. *J. Am. Chem. Soc.***2008**, *130*, 1477; c) Hutchings, G. J. *Chem. Commun.* **2008**, 1148; d) Shin, J.; Kim, H.; Lee, I. S. *Chem. Commun.* **2008**, 5553; e) George, C.; Dorfs, D.; Bertoni, G.; Falqui, A.; Genovese, A.; Pellegrino, T.; Roig, A.; Quarta, A.; Comparelli, R.; Curri, M. L.; Cingolani, R.; Manna, L. *J. Am. Chem. Soc.* **2011**, *133*, 2205.

12. a) Gu, H.; Yang, Z.; Gao, J.; Chang, C. K.; Xu, B. *J. Am. Chem. Soc.* **2005**, *127*, 34; b) Li, Y.; Zhang, Q.; Nurmikko, A. V.; Sun, S. *Nano Lett.* **2005**, *5*,

1689; c) Yu, H.; Chen, M.; Rice, P. M.; Wang, S. X.; White, R. L.; Sun, S. *Nano Lett.* **2005**, *5*, 379; d) Choi, S. H.; Na, H. B.; Park, Y. I.; An, K.; Kwon, S. G.; Jang, Y.; Park, M. H.; Moon, J.; Son, J. S.; Song, I. C.; Moon, W. K.; Hyeon, T. *J. Am. Chem. Soc.* **2008**, *130*, 15573; e) Xu, C.; Xie, J.; Ho, D.; Wang, C.; Kohler, N.; Walsh, E. G.; Morgan, J. R.; Chin, Y. E.; Sun, S. *Angew. Chem. Int. Ed* **2008**, *47*, 173.

13. Jang, Y.; Chung, J.; Kim, S.; Jun, S. W.; Kim, B. H.; Lee, D. W.; Kim, B. M.; Hyeon, T. *Phys. Chem. Chem. Phys.* **2011**, *13*, 2512.

14. Chung, J.; Kim, J.; Jang, Y.; Byun, S.; Hyeon, T.; Kim, B. M. *Tetrahedron Lett.* **2013**, *54*, 5192.

15. Lee, J.; Chung, J.; Byun, S. M.; Kim, B. M.; Lee, C. *Tettrahedron* **2013**, *69*, 5660.

16. Byun, S.; Chung, J.; Jang, Y.; Kwon, J.; Hyeon, T.; Kim, B. M. *RSC Advances* **2013**, *3*, 16296.

17. Zhang, R.; Miao, C.-X.; Wang, S.; Xia, C.; Sun, W. *ChemCatChem* **2012**, *4*, 192.

18. a) Biffis, A.; Zecca, M.; Basato, M.*Eur. J. Inorg. Chem.* **2001**, 1131; b) Phan, N. T. S.; Van Der Sluys, M.; Jones, C. W. *Adv. Synth. Catal.* **2006**, *348*, 609.

19. Crabtree, R. H. *Chem. Rev.* **2012**, *112*, 1536.

20. Son, S. U.; Jang, Y.; Park, J.; Na, H. B.; Park, H. M.; Yun, H. J.; Lee, J.; Hyeon, T. *J. Am. Chem. Soc.* **2004**, *126*, 5026.

21. Teranishi, T.; Wachi, A.; Kanehara, M.; Shoji, T.; Sakuma, N.; Nakaya, M. *J. Am. Chem. Soc.* **2008**, *130*, 4210

Part I. Chapter 2

1. a) Campbell, K.N.;Campbell, B.K.*Chem. Rev.* **1942**, *31*, 77; b) Burwell Jr. R. L.*Chem. Rev.* **1957**, *57*, 895; c) Bond, G. C.; Wells, P.B.*Adv. Catal.* **1964**, *15*, 91; d) Marvell, E.N.; Li,T. *Synthesis* **1973**, 457.

2. a) Blaser, H.-U.; Indolese, A.;Schnyder, A.;Steiner, H.; Studer, M.*J. Mol. Catal. A* **2001**, *173*, 3; b) Domínguez-Domínguez, S.; Berenguer-Murcia, Á.; Pradhan, B. K.; Linares-Solano, Á.; Cazorla-Amorós, D.*J. Phys. Chem. C* **2008**, *112*, 3827.

3. a) Lindlar,H.; Dubuis, R.*Org. Synth.* **1966**, *46*, 89; b) Lindlar, H.; Dubuis, R.*Org. Synth. Colloids* **1973**, *5*, 880; c) Rajaram, J.; Narula, A. P. S.; Chawla,H. P. S.; Dev, S. *Tetrahedron* **1983**, *39*,2315; d) Ghosh,A. K.; Krishnan,K. *Tetrahedron Lett.* **1998**, *39*, 947.

4. a) Wovkulich, P. M.; Baggiolini, E. G.; Heenessy, B. M.; Uskoković,M. R.*J. Org. Chem.* **1983**, *48*, 4436; b) Ulan, J. G.; Maier, W. F.; Smith, D. A.*J. Org. Chem.* **1987**, *52*, 3132.

5. Lee, K. H.; Lee, B.; Lee, K. R.; Yi, M. H.; Hur, N. H. *Chem. Commun.* **2012**, *48*, 4414.

6. a) Narayanan, R.; El-Sayed, M. A.*Nano Lett.* **2004**, *4*, 1343; b) Habas, S. E.; Lee, H.;Radmilovic, V.; Somorjai, G. A.; Yang, P. *Nat. Mater.* **2007**, *6*, 692; c) Wang, C.; Daimon, H.; Onodera, T.; Koda, T.; Sun,S. *Angew. Chem.* **2008**, *120*, 3644; *Angew. Chem. Int. Ed.* **2008**, *47*, 3588; d) Zhang, Y.; Grass, M. E.; Kuhn, J. N.; Tao, F.; Habas, S. E.; Huang, W.; Yang, P.; Somorjai, G. A.*J. Am. Chem. Soc*. **2008**, *130*, 5868; e) Mori, S.; Ohkubo, T.; Ikawa, T.; Kume, A.; Maegawa, T.; Monguchi, Y.; Sajiki, H.*J. Mol. Catal. A: Chem.* **2009**, *307*, 77; f) Semagina, N.; Kiwi-Minsker, L.*Catal. Lett.* **2009**,

127, 334; g) Tsung, C.-K.; Kuhn, J. N.; Huang, W.; Aliaga, C.; Hung, L.-I.; Somorjai, G. A.; Yang, P.*J. Am. Chem. Soc*. **2009**, *131*, 5816.

7. Lim, B.; Jiang, M.; Tao, J.; Camargo, P. H. C.; Zhu, Y.; Xia, Y. *Adv. Funct. Mater.* **2009**, *19*, 189.

8. a) Gentle, T. M.; Muettertles, E. L.*J. Phys. Chem*. **1983**, *87*, 2469; b) Dunphy, J. C.; Rose, M.; Behler, S.; Ogletree, D. F.; Salmeron, M.*Phys. Rev. B***1998**, *57*, 705; c) Vattuone, L.; Yeo, Y. Y.; Kose, R.; King, D. A.*Surf. Sci*. **2000**, *447*, 1; d) Mittendorfer, F.; Thomazeau, C.; Raybaud, P.; Toulhoat, H.*J. Phys. Chem. B* **2003**, *107*, 12287.

9. Yang, D.; Xia, L.; Zhao, H.; Hu, X.; Liu, Y.; Li, J.; Wan, X.*Chem. Commun*, **2011**, *47*, 5873.

10. Crespo-Quesada, M.; Yarulin, A.; Jin, M.; Xia,Y.; Kiwi-Minsker, L. *J. Am. Chem. Soc*. **2011**, *133*, 12787.

11. a) Mitsudome, T.; Takahashi, Y.; Ichikawa, S.; Mizugaki, T.; Jitsukawa, K.; Kaneda, K. *Angew. Chem. Int. Ed* **2013**, *52*, 1481; b) Ulan, J. G. ; Maier, W. F.; Smith, D. A.*J. Org. Chem.* **1987**, *52*, 3132;

12. a) Kresse,G.; Furthmüller, J. *Phys. Rev. B: Condens. Matter Mater. Phys.* **1996**, *54*, 11169; b) Kresse,G.; Furthmüller, J. *Comput. Mater. Sci*. **1996**, *6*, 15.

13. Kresse, G.; Hafner, J.*J. Phys.: Condens. Matter* **1994**, *6*, 8245.

14. Perdew, J. P.; Chevary, J. A.; Vosko, S. H.; Jackson, K. A.; Pederson,M. R.; Singh, D. J.; Fiolhais, C. *Phys. Rev. B: Condens. Matter Mater. Phys.* **1992**, *46*, 6671.

Part II

1. a) Fuhrmann, T.; Salbeck, J. *Mrs Bull* **2003**, *28*, 354; b) Komoda, T.; Ide, N.; Kido, J. *J. Light & Visual Environment* **2008**, *32*, 75.

2. a) Gross, M.; Muller, D. C.; Nothofer, H. G.; Scherf, U.; Neher, D.; Brauchle, C.; Meerholz, K. *Nature* **2000**, *405*, 661; b) Chwang, A. B.; Rothman, M. A.; Mao, S. Y.; Hewitt, R. H.; Weaver, M. S.; Silvernail, J. A.; Rajan, K.; Hack, M.; Brown, J. J.; Chu, X.; Moro, L.; Krajewski, T.; Rutherford, N. *Appl. Phy. Lett.* **2003**, *83*, 413; c) Kelley, T. W.; Baude, P. F.; Gerlach, C.; Ender, D. E.; Muyres, D.; Haase, M. A.; Vogel, D. E.; Theiss, S. D. *Chem. Mater.* **2004**, *16*, 4413; d) Zhou, L.; Wanga, A.; Wu, S.-C.; Sun, J.; Park, S.; Jackson, T. N. *Appl. Phy. Lett.* **2006**, *88*, 083502.

3. a) Lee, M. T.; Liao, C. H.; Tsai, C. H.; Chen, C. H. *Adv.Mater.* **2005**, *17*, 2493; b) Sun, Y.; Giebink, N. C.; Kanno, H.; Ma, B.; Thompson, M. E.; Forrest, S. R. *Nature* **2006**, *440*, 908; c) Reineke, S.; Baldo, M. A. *physica status solidi (a)* **2012**, *209*, 2341.

4. a) Lamansky, S.; Djurovich, P.; Murphy, D.; Abdel-Razzaq, F.; Lee, H.-E.; Adachi, C.; Burrows, P. E.; Forrest, S. R.; Thompson, M. E. *J. Am. Chem. Soc.* **2001**, *123*, 4304; b) Yeh, S. J.; Wu, M. F.; Chen, C. T.; Song, Y. H.; Chi, Y.; Ho, M. H.; Hsu, S. F.; Chen, C. H. *Adv. Mater.* **2005**, *17*, 285; c) Ding, J.; Gao, J.; Cheng, Y.; Xie, Z.; Wang, L.; Ma, D.; Jing, X.; Wang, F. *Adv. Funct. Mater.* **2006**, *16*, 575.

5. a) Xiao, L.; Chen, Z.; Qu, B.; Luo, J.; Kong, S.; Gong, Q.; Kido, J. *Adv. Mater.* **2011**, *23*, 926; b) Yook, K. S.; Lee, J. Y. *Adv. Mater.* **2012**, *24*, 3169.

6. a) Su, S.-J.; Sasabe, H.; Takeda, T.; Kido, J. *Chem. Mater.* **2008**, *20*, 1691; b) Hsu, F.-M.; Chien, C.-H.; Shu, C.-F.; Lai, C.-H.; Hsieh, C.-C.; Wang, K.-W.; Chou, P.-T. *Adv. Funct. Mater.* **2009**, *19*, 2834; c) Chou, H. H.; Cheng, C. H. *Adv. Mater.* **2010**, *22*, 2468; d) Ananth Reddy, M.; Thomas, A.; Mallesham,

G.; Sridhar, B.; Jayathirtha Rao, V.; Bhanuprakash, K. *Tetrahedron Lett.* **2011**, *52*, 6942; e) Chaskar, A.; Chen, H. F.; Wong, K. T. *Adv. Mater.* **2011**, *23*, 3876; f) Fan, C.; Zhao, F.; Gan, P.; Yang, S.; Liu, T.; Zhong, C.; Ma, D.; Qin, J.; Yang, C. *Chemistry* **2012**, *18*, 5510; g) Hung, W.-Y.; Tu, G.-M.; Chen, S.-W.; Chi, Y. *J. Mater. Chem.* **2012**, *22*, 5410.

국문초록

I. 팔라듐 나노결정를 이용한 효과적인 유기 반응 개발

유기 합성 분야에 있어서 팔라듐은 다양한 작용기 변환 반응과 탄소-탄소 결합 반응에 이용되는 가장 중요한 금속 촉매이다. 그러나 이러한 팔라듐 촉매 반응의 중요함에도 불구하고 균일상 팔라듐 촉매를 이용하는 반응들은 공기중의 불안정성, 생성물 속의 잔여 금속, 안전, 비용 등의 문제를 동반하게 된다. 이러한 단점들은 균일상 팔라듐 촉매의 산업화에 큰 저해가 되고 있다. 이와 같은 단점들을 해결하기 위해서 연구자들은 불균일 팔라듐 촉매를 개발했다. 그러나 불균일 촉매는 균일상 촉매에 비교하여 반응성이나 선택성이 떨어지는 문제를 겪고 있다. 그로 인해 불균일 촉매는 반응의 적용범위가 좁고 더 강한 실험 조건을 필요로 하게 된다. 그러므로 이러한 불균일 촉매와 균일 촉매의 단점을 줄이고 장점을 극대화시킬 수 있는 새로운 형태의 촉매 개발이 필요하다. 이러한 목표를 이룰 수 있는 방법으로 많은 연구자들은 나노 결정을 촉매로 이용하는 방법을 제시하고 있다. 나노 결정은 부피 대비 높은 면적 비율과 좋은 분산성을 가지고 있어 균일 촉매와 같은 높은 반응성을 기대할 수 있다. 게다가 나노 결정은 기본적으로 불균일 촉매와 같은 방식으로 쉽게 취급이 가능하다. 이러한 특징덕분에 나노 결정 촉매반응은 반불균일질 촉매 반응이라고도 불리며 균일질 촉매와 불균일 촉매 양쪽 모두의 장점을 가지고 있다. 그 예로 균일질 촉매의 높은 반응 효율과 불균일 촉매의 재사용성을 동시에 가지고 있는 나노 결정 촉매를 들 수 있다.

첫 번째 장에서는 자성으로 분리가능하며 여과를 필요로 하지 않는 팔라듐-산화철 나노 결정 촉매의 이용법과 적용 사례를 보고하고

자 한다. 팔라듐-산화철 나노 결정 촉매는 교차 결합 반응에 효과적이며 매번 반응을 수행한 후, 자성을 이용하여 혼합물로부터 쉽게 회수가 가능하다. 회수한 촉매는 다양한 유기 반응에서 보존된 좋은 반응성을 보이며 여러 번의 재사용이 가능한 것으로 드러났다. 이러한 효과적이고 간단하며 환경친화적인 팔라듐 나노 결정 촉매는 대량 합성에도 적용할 수 있어 실제 공정이나 산업화에도 유용할 것으로 기대된다. 이러한 나노 촉매를 응용하는 기술의 더 큰 가능성과 실제 작용기작에 대해서 밝혀내기 위하여 현재 노력중에 있다.

두 번째 장에서는 금속 나노 결정의 형태 조절에 의한 반응성 변화에 대하여 보고하고자 한다. 금속 나노 결정의 촉매적인 성질은 표면의 원자 배치와 같은 형태에 의해서 변화하는 것으로 드러나 있는데 이것은 특정 반응에서의 효율성이나 선택성을 조절 가능한 것으로 기대된다. 이를 바탕으로 우리는 금속의 면 배열을 조절하여 알카인의 수소화 반응에 선택성을 부여할 수 있다는 결과를 밝혀내었다. 정육면체의 형태로 합성된 팔라듐 나노 결정은 {100}의 면배열을 가지며 이 나노 결정을 다양한 알카인의 수소화 반응에 적용한 결과 선택적으로 알케인을 합성할 수 있었다. 이러한 팔라듐 나노 결정의 형태 조절에 기반한 우리의 연구 접근 방법은 알카인의 선택적 환원반응에 간단하게 높은 선택성을 부여할 수 있는 것으로 밝혀졌다.

II. 유기 발광 다이오드에 응용 가능한 신규 청색 인광 호스트 물질의 설계 및 합성

유기 발광 다이오드 기술은 모든 색을 배출할 수 있으며 낮은 구동전압과 높은 반응 속도, 적은 전력 소비 등의 장점을 갖추고 있어 차세대 조명 및 디스플레이 기술로 손꼽히고 있다. 유기 발광 다이

오드는 자기 발광 성질을 가지고 있어 추가적인 후면광을 필요로 하지 않는다는 장점도 가지고 있다. 이러한 유기 발광 다이오드를 이용한 소자는 1 밀리미터 이내의 두께로 제작이 가능한데 이것은 현재 주로 사용되는 액정 표시 장치의 소자보다도 훨씬 얇은 두께에 해당된다. 게다가 유기 발광 다이오드는 쉬운 제조 공정으로 생산이 가능하며 신축성을 가진 휴대용 디스플레이에도 적용이 가능할 것으로 기대된다.

그러나 이러한 유기 발광 다이오드 기술은 높은 삼중항 에너지를 가지면서 안정한 청색 인광물질을 필요로 한다. 그러나 효과적으로 합성가능하며 높은 에너지 전달 효율을 가진 청색 인광 호스트 소재는 개발을 필요로 한다. 이에 본 연구에서는 호스트 물질로 사용 가능한 신규 청색 인광물질의 설게 및 합성을 수행하였다. 특히 전자를 주는 성질의 작용기와 전자를 잘 받아주는 성질의 작용기가 한 분자 내에 결합된 양극성 물질 구조의 분자를 주요 목표로 하였다. 합성된 분자들은 소자 평가 결과 발광 효율은 평범한 수준이었으나 좋은 색 좌표 값을 보여주었다.